UNIVERSIDAD DE CONCEPCIÓN

Centro de Investigación en Ingeniería Matemática (CI^{2}MA)

An unfitted HDG discretization for a model problem in shape optimization

Esteban Henriquez, Tonatiuh Sanchez-Vizuet,
Manuel Solano

PREPRINT 2025-21

SERIE DE PRE-PUBLICACIONES

An unfitted HDG discretization for a model problem in shape optimization

Esteban Henríquez*[1], Tonatiuh Sánchez-Vizuet†[2], and Manuel Solano‡[3,4]

[1]Department of Applied Mathematics, University of Waterloo, Ontario, Canada.
[3]Departamento de Ingeniería Matemática, Facultad de Ciencias Físicas y Matemáticas, Universidad de Concepción, Concepción, Chile.
[4]Center for Research in Mathematical Engineering CI[2]MA, Universidad de Concepción, Concepción, Chile.
[2]Department of Mathematics, The University of Arizona, USA.

September 29, 2025

Abstract

We apply an unfitted HDG discretization to a model problem in shape optimization. The method proposed uses a fixed, shape regular, non-geometry conforming mesh and a high order transfer technique to deal with the curved boundaries arising in the optimization process. The use of this strategy avoids the need for constant remeshing and enables a highly accurate description of the domain using a coarse computational mesh. We develop a rigorous analysis of the well-posedness of the problems that arise from the optimality conditions, and provide an *a priori* error analysis for the resulting discrete schemes. Numerical examples with manufactured problems are provided demonstrating the convergence of the scheme and the efficiency of the transfer path method. The approach proposed yields high resolution approximations of the boundary using grids with as few as 100 times less elements than an interpolatory technique.

Keywords: Shape optimization; hybridyzable discontinuous Galerkin; transfer path method.

Mathematics Subject Classification (2020) 49M41, 65N30.

==========

1 Introduction

Shape optimization is an important branch of the study of optimal control theory, which was developed extensively in the 1990s and arises from the need to minimize a quantity (for instance the amount of material needed to build an industrial component or the energy cost of production) through the modification of the design shape. This area has inspired the development of a wide variety of theoretical and purely mathematical tools and has a large number of applications in science and engineering, such as architecture and civil engineering [5], fluid mechanics [16, 33, 60], modeling of quantum chemistry phenomena [8, 12], electromagnetism or photonics [40, 42], among other research fields. From a mathematical point of view, we can see shape optimization as finding the minimum (possibly local) of a cost functional defined over a set of admissible domains. In many cases—and we shall focus on these—the minimization problem is constrained by a partial differential equation (PDE) defined on the target domain. The computation of this minimum often requires the repeated solution of further partial differential equations arising from the optimality conditions associated to the functional in question.

The first Discontinuous Galerkin (DG) method was developed in 1973 by Reed and Hill in the context of a neutron transport problem involving a linear, time-independent, hyperbolic equation [50]. Since then, DG methods have become one of the most widely used tools for the numerical solution of PDEs. However, DG discretizations were criticized due to the fact that the associated linear systems involve too many unknowns and involve a complicated

*ehenriqu@uwaterloo.ca
†tonatiuh@arizona.edu
‡msolano@ing-mat.udec.cl

computational implementation compared to Continuous Galerkin (CG) methods. These criticisms were resolved after the development of Hybridizable Discontinuous Galerkin (HDG) methods, first for diffusion problems and later presented in a unified framework [21].

During the last two decades, HDG methods have been extensively developed for different types of equations, for instance, diffusion equations [19, 22, 23, 41], convection-diffusion equations [20, 34, 48], acoustic and elastic waves [4, 25], Stokes flow [13, 27, 35, 43], Oseen and Brinkman equations [3, 14, 36], Navier-Stokes equations [15, 47, 51], linear and nonlinear elasticity [28, 46, 59], just to name a few.

In recent years, the development of the *transfer path method* has allowed the application of HDG to domains that are not necessarily polygonal/polyhedral by approximating the solution in a polygonal subdomain. This transfer technique was introduced within the context of HDG discretizations for linear elliptic equations in [24, 29] and allows for the use of simple polygonal, non-interpolating meshes while still maintaining high order of convergence. Since then, this method has been used for Stokes flow [57], Oseen equations [58], the Helmholtz equation [11], convection diffusion equations [30], the Grad-Shafranov equation [55, 56], coupling with integral equations [26], non-linear problems [52, 53, 54], and recently for a distributed optimal control problem [38], among others.

For the treatment of partial differential equations arising from the shape optimization problem, work has been carried out using a variety of methods, for instance, Finite Element Method (FEM) [32], Cut Finite Element Methods (CutFEM) [9, 10], Boundary Element Method (BEM) [7, 45], level-set methods [1, 2], among others. For this manuscript we seek to make a first approach in using the combination of the transfer path method with an HDG discretization to deal with the curved domains that arise naturally in shape optimization problems. These techniques combined shall allow for the use of simple, shape regular triangulations, while maintaining the high order of convergence of these methods in this new context.

In Section 2 we introduce a model problem and derive the optimality conditions associated to the optimization problem as well as the optimization algorithms at the continuous level. Section 3 is devoted to the introduction of the transfer path method and the technical assumptions related to the geometry and triangulation. The unfitted HDG discretizations of the state, adjoint and deformation variables are introduced in Section 4, followed by the corresponding *a priori* error analysis in Section 5. Finally, using manufactured examples, Section 6 presents numerical experiments showcasing the convergence of the discrete variables and the behavior of the suggested shape–optimization algorithm.

2 The model problem

Let $\mathcal{U} \subset \mathbb{R}^d$ be a fixed domain, $\mu(\cdot)$ denote the Lebesgue measure in $\mathbb{R}^n$, and define the set

$$\mathcal{O} := \{\Omega : \Omega \subset \mathcal{U} \ \text{ and } \ \mu(\Omega) = m_0\} \ .$$

We will refer to any $\Omega \in \mathcal{O}$ as an *admissible domain* and will denote its boundary as $\Gamma := \partial\Omega$. For a fixed *target function* $\widetilde{y} \in H^1(\mathcal{U})$ we will define the energy functional $J : \mathcal{O} \times H^1(\mathcal{U}) \to \mathbb{R}$ as

$$J(\Omega; y) := \frac{1}{2} \int_\Omega (y - \widetilde{y})^2.$$

In this work we will consider the model problem of finding a domain $\widehat{\Omega} \in \mathcal{O}$ such that

$$\left(\widehat{\Omega}, y\right) = \underset{\Omega \in \mathcal{O}}{\arg\min}\, J\left(\Omega; y\right) \tag{1}$$

where the function y is subject to the *state equation*

$$-\nabla \cdot (a \nabla y) = f \quad \text{in } \Omega\,, \tag{2a}$$

$$y = g \quad \text{on } \Gamma. \tag{2b}$$

Above, the scalar function a is assumed to be such that there exist real numbers $\underline{a}$ and $\overline{a}$ satisfying

$$0 < \underline{a} \leq a \leq \overline{a} < \infty \qquad \text{almost everywhere on } \mathcal{U}\,,$$

and $f \in H^1(\mathcal{U})$ and $g \in H^2(\mathcal{U})$ are given problem data. Note that, since y is defined as the solution of a PDE defined on Ω, it is itself a function of Ω. To keep notation as light as possible, we will avoid denoting this fact explicitly as $y(\Omega)$, but the reader should keep this dependence in mind.

If we consider a Lipschitz mapping $\boldsymbol{V} : \mathcal{U} \to \mathbb{R}^d$ and small deformations of the domain Ω of the form

$$\Omega \ni \boldsymbol{x} \mapsto \boldsymbol{x} + \epsilon \boldsymbol{V}(\boldsymbol{x}) \qquad \text{for } 0 < \epsilon < 1,$$

the variation $\delta J(\Omega; \boldsymbol{V})$ of the functional $J(\Omega; y)$ can be characterized (cf. [44, Chapter 11]) in terms of the problem data, g and $\widetilde{y}$, and the *adjoint function* z, as

$$\delta J(\Omega; \boldsymbol{V}) \;=\; \int_\Gamma G(\Gamma)\, \boldsymbol{V} \cdot \boldsymbol{n}, \tag{3}$$

where

$$G(\Gamma) := \, a\, \partial_{\boldsymbol{n}} z\, \partial_{\boldsymbol{n}} (y \,-\, g) \,+\, \frac{1}{2} (g \,-\, \widetilde{y})^2 \,, \tag{4}$$

and $z \in H^2(\Omega)$ is the solution to the *adjoint problem*

$$\begin{aligned} -\nabla \cdot (a\, \nabla z) \;&=\; y \,-\, \widetilde{y} \qquad && \text{in } \Omega \,, \\ z \;&=\; 0 \qquad && \text{on } \Gamma \,. \end{aligned} \tag{5}$$

Therefore, we look for a domain $\widehat{\Omega}$ that satisfies $\delta J(\widehat{\Omega}; \boldsymbol{V}) \,=\, 0$ for some admissible direction $\boldsymbol{V}$ that we will call the *deformation field* and will be specified below.

It is known [39] that shape optimization problems generally do not have a unique solution because the optimality condition $\delta J(\widehat{\Omega}; \boldsymbol{V}) \,=\, 0$ does not uniquely determine $\boldsymbol{V}$. For instance, to first order, deformations in the direction tangential to Γ will not affect the value of the functional. Hence, a common choice is to fix a small portion, Γ_D, of the boundary and to look for a deformation field that satisfies

$$\begin{aligned} -\Delta \boldsymbol{V} \;&=\; \boldsymbol{0} \qquad && \text{in } \Omega, \\ \partial_{\boldsymbol{n}} \boldsymbol{V} \;&=\; -\, G(\Gamma)\, \boldsymbol{n} \qquad && \text{on } \Gamma_N, \\ \boldsymbol{V} \;&=\; \boldsymbol{0} \qquad && \text{on } \Gamma_D, \end{aligned} \tag{6}$$

where Γ_N is the piece of the boundary that can be deformed and Γ_D is the piece of the boundary that will remain fixed and $\Gamma = \Gamma_D \cup \Gamma_N$. We will assume that $\mu(\Gamma_N) \,\neq\, 0$ and $\mu(\Gamma_D) \,\neq\, 0$.

The space

$$[H_D(\Omega)]^d \,:=\, \{\boldsymbol{w} \in [H^1(\Omega)]^d, \quad \boldsymbol{w} \,=\, \boldsymbol{0} \text{ on } \Gamma_D\}.$$

will be used to enforce the Dirichlet boundary condition in the weak formulation for the problem (6), which we can now state as

$$\begin{aligned} &\text{Find } \boldsymbol{V} \in [H_D(\Omega)]^d \quad \text{such that} \\ &\int_\Omega \nabla \boldsymbol{V} : \nabla \boldsymbol{w} + \int_{\Gamma_N} G(\Gamma)\, \boldsymbol{w} \cdot \boldsymbol{n} \,=\, 0 \quad \forall\, \boldsymbol{w} \in [H^1_D(\Omega)]^d \,. \end{aligned} \tag{7}$$

Here, for any tensor fields $\boldsymbol{\psi} \,=\, (\psi_{ij})_{i,j=1,n}$ and $\boldsymbol{\zeta} \,=\, (\zeta_{ij})_{i,j=1,n}$, the tensor inner product is defined as

$$\boldsymbol{\psi} : \boldsymbol{\zeta} \,=\, \sum_{i=1}^{n} \sum_{j=1}^{n} \psi_{ij}\, \zeta_{ij}.$$

Thus, by letting $\boldsymbol{w} \,=\, \boldsymbol{V}$, it follows from the weak formulation (7) and equation (3) that

$$\delta J(\Omega; \boldsymbol{V}) \;=\; \int_{\Gamma_N} G(\Gamma)\, \boldsymbol{V} \cdot \boldsymbol{n} \;=\; -\int_\Omega |\nabla \boldsymbol{V}|^2 \;\leq 0 \,, \tag{8}$$

which implies that deformations of Ω in a direction $\boldsymbol{V}$ that satisfies (6) guarantee a decrease in the value of the functional. Note that this is not the only possible choice for $\boldsymbol{V}$, but we will stick to it for the remainder of this work.

The previous argument motivates the following algorithm to compute an approximation for Ω^{opt} based on the gradient descent method [44, Algorithm 11.1]. Starting from an initial guess $\Omega^{(0)}$, the approximation can be updated iteratively as

$$\Omega^{(k+1)} \;=\; (I \,+\, \tau_k \, \boldsymbol{V}^{(k)})\Omega^{(k)} \quad (k \in \mathbb{N})\,,$$

where τ_k is a scalar parameter, referred to as the *step size*, that controls the size of the deformation (its precise value will be determined later) and the descent direction $\boldsymbol{V}^{(k)}$ is the solution to

$$-\,\Delta \boldsymbol{V}^{(k)} = \boldsymbol{0} \qquad \text{in } \Omega^{(k)}, \tag{9a}$$

$$\partial_{\boldsymbol{n}} \boldsymbol{V}^{(k)} = -\; G(\Gamma^{(k)})\, \boldsymbol{n} \qquad \text{on } \Gamma_N^{(k)}, \tag{9b}$$

$$\boldsymbol{V}^{(k)} = \boldsymbol{0} \qquad \text{on } \Gamma_D^{(k)}. \tag{9c}$$

Analogously to (8) we can prove that $\boldsymbol{V}^{(k)}$ is a descent direction for each $k \in \mathbb{N}$, and therefore

$$J(\Omega^{(k+1)}, y^{(k+1)}) \;\leq\; J(\Omega^{(k)}, y^{(k)}) \quad \forall\, k \in \mathbb{N}\,.$$

Generating the Neumann data for the problem above requires the successive solution of the state equation (2) and the adjoint equation (5) at every iteration. The process can be repeated until the value of the functional falls below a predetermined tolerance $\text{TOL} > 0$.

In summary, given an initial guess for the domain $\Omega^{(0)}$ and a desired tolerance TOL for the value of the functional $J(\Omega, y)$ the sequence of steps to obtain an approximation to the shape optimal shape, is

Algorithm 1 [44, Algorithm 11.1]

Require: Initial domain $\Omega^{(0)}$ and tolerance parameter TOL
  $y^{(0)} \leftarrow y(\Omega^{(0)})$ by solving the state equation (cf. (2)) in $\Omega^{(0)}$
  $z^{(0)} \leftarrow z(\Omega^{(0)})$ by solving the adjoint equation (cf. (5)) in $\Omega^{(0)}$
  compute $J(\Omega^{(0)})$
  compute $G(\Gamma^{(0)})$
  compute a deformation field $\boldsymbol{V}^{(0)}$ by solving (9)
  $k \leftarrow 0$
  while $|\delta J(\Omega^{(k)}; \boldsymbol{V}^{(k)})/\delta J(\Omega^{(0)}; \boldsymbol{V}^{(0)})| > \text{TOL}$ **or** $|J(\Omega^{(k)}) - J(\Omega^{(k-1)})| > \text{TOL}$ **do**
    compute the step size parameter τ_k with a line search routine
    $\Omega^{(k+1)} \leftarrow (I + \tau_k \boldsymbol{V}^k)(\Omega^{(k)})$
    $y^{(k+1)} \leftarrow y(\Omega^{(k+1)})$ by solving the state equation (2) in $\Omega^{(k+1)}$
    $z^{(k+1)} \leftarrow z(\Omega^{(k+1)})$ by solving the adjoint equation (5) in $\Omega^{(k+1)}$
    compute $J(\Omega^{(k+1)})$
    compute $G(\Gamma^{(k+1)})$
    compute a deformation field $\boldsymbol{V}^{(k+1)}$ by solving (9)
    $k \leftarrow k + 1$
  end while

In practice, the *volume constraint* on the admissible domains $\mu(\Omega) = m_0$ can be challenging to enforce computationally. Thus, we follow [44, Section 11.5.1], and introduce a Lagrange multiplier ξ and the functional

$$\widetilde{J}(\Omega, \xi; y) := J(\Omega; y) + \xi(\mu(\Omega) - m_0).$$

The variation $\delta\widetilde{J}(\Omega, \xi; \boldsymbol{V})$ of the functional $\widetilde{J}(\Omega, \xi; y)$ can be characterized by

$$\delta\widetilde{J}(\Omega, \xi; \boldsymbol{V}) = \delta J(\Omega; \boldsymbol{V}) + \xi \int_\Gamma \boldsymbol{V} \cdot \boldsymbol{n} = \int_\Gamma \widetilde{G}(\Gamma, \xi)\boldsymbol{V} \cdot \boldsymbol{n},$$

where $\widetilde{G}(\Gamma, \xi) := G(\Gamma) + \xi$. We compute $\boldsymbol{V}$ by solving (6) using the quantity $-\widetilde{G}(\Gamma)\boldsymbol{n}$ as a Neumann boundary condition. In addition, the Lagrange multiplier is updated every iteration according to

$$\xi^{(k+1)} = \frac{\xi^{(k)} + \chi(\Gamma)}{2} + \epsilon(\mu(\Omega) - m_0), \quad \text{with} \quad \chi(\Gamma) := -\frac{1}{\mu(\Gamma)} \int_\Gamma G(\Gamma)\,, \tag{10}$$

and $\epsilon > 0$ a sufficiently small fixed constant. This leads to the following modified algorithm:

Algorithm 2 Modification of Algorithm 1

Require: Initial domain $\Omega^{(0)}$, parameters TOL and ϵ
$y^{(0)} \leftarrow y(\Omega^{(0)})$ by solving the state equation (cf. (2)) in $\Omega^{(0)}$
$z^{(0)} \leftarrow z(\Omega^{(0)})$ by solving the adjoint equation (cf. (5)) in $\Omega^{(0)}$
compute $\chi(\Gamma^{(0)})$ and set $\xi^{(0)} := \chi(\Gamma^{(0)})$
compute $\widetilde{J}(\Omega^{(0)}, \xi^{(0)})$
compute $\widetilde{G}(\Gamma^{(0)}, \xi^{(0)})$
compute a deformation field $\boldsymbol{V}^{(0)}$ by solving (9) with $\widetilde{G}(\Gamma^{(0)}, \xi^{(0)})$ as Neumann boundary data
$k \leftarrow 0$
while $|\delta\widetilde{J}(\Omega^{(k)}, \xi^{(k)}; \boldsymbol{V}^{(k)})/\delta\widetilde{J}(\Omega^{(0)}, \xi^{(0)}; \boldsymbol{V}^{(0)})| >$ TOL **or** $|\widetilde{J}(\Omega^{(k)}, \xi^{(k)}) - \widetilde{J}(\Omega^{(k-1)}, \xi^{(k-1)})| >$ TOL **do**
  for a fixed $\xi^{(k)}$, compute the step size parameter τ_k by a line search routine.
  $\Omega^{(k+1)} \leftarrow (I + \tau_k \boldsymbol{V}^k)(\Omega^{(k)})$
  $y^{(k+1)} \leftarrow y(\Omega^{(k+1)})$ by solving the state equation (2) in $\Omega^{(k+1)}$
  $z^{(k+1)} \leftarrow z(\Omega^{(k+1)})$ by solving the adjoint equation (5) in $\Omega^{(k+1)}$
  compute $\chi(\Gamma^{(k+1)})$ and set $\xi^{(k+1)} = \dfrac{\xi^{(k)} + \chi(\Gamma^{(k+1)})}{2} + \epsilon(\mu(\Omega^{(k+1)}) - m_0)$
  compute $\widetilde{J}(\Omega^{(k+1)}, \xi^{(k+1)})$
  compute $\widetilde{G}(\Gamma^{(k+1)}, \xi^{(k+1)})$
  compute a deformation field $\boldsymbol{V}^{(k+1)}$ by solving (9) with $\widetilde{G}(\Gamma^{(k+1)}, \xi^{(k+1)})$ as Neumann boundary data
  $k \leftarrow k + 1$
end while

3 Unfitted geometric discretization

In addition to the solution to three boundary value problems at every step, Algorithm 1 requires the update of the domain $\Omega^{(k)}$ where the state, adjoint, and deformation equations will be posed on the next iteration. For many numerical schemes, this poses the need to repeatedly generate a new computational mesh. This requirement can render an algorithm too costly, especially if the iteration count is high—which is typically the case. Moreover, to achieve a highly accurate approximation of Ω^{opt}, traditional methods would require either the use of an extremely fine interpolatory mesh, or an isogeometric triangulation, or a high order curvilinear mesh. All of these methods can produce a precise description of the target geometry, but they achieve so at an additional computational cost per step that may result unacceptable if the iteration count is high—which is typically the case.

Due to these particularities, the transfer path method [24, 29]—that we describe below—provides an ideal tool for dealing with this iterative process, as it obviates both the need to create a new mesh with every successive iteration and the requirement of a mesh that finely captures the geometric properties of the boundary $\Gamma^{(k)}$. These characteristics can dramatically decrease the additional costs associated with the geometric approximation. The aim of this paper is to propose and analyze unfitted HDG discretizations that take advantage of the transfer path method for the three relevant equations in the process. Here, we describe the geometric setting for the computations and the transfer path method.

The computational domain
We will assume that the domain Ω has a Lipschitz boundary Γ and will choose a background polyhedral domain $\mathcal{M}$ such that $\Omega \subset \overline{\mathcal{U}} \subset \overline{\mathcal{M}}$. We will denote a generic triangulation (or tetrahedrization, depending on the dimension) of $\mathcal{M}$ by T_h and a generic element in the triangulation by K. As usual, we will denote

$$h := \max_{K \in T_h} \{\text{diam}(K)\} \qquad \text{and} \qquad \underline{h} := \min_{K \in T_h} \{\text{diam}(K)\}.$$

We refer to T_h as a *background triangulation* and define

$$\mathcal{T}_h := \{K \in T_h : K \subset \overline{\Omega}\}, \tag{11}$$

i.e. the set of all the elements $K \in T_h$, which are completely contained in Ω. For any given background triangulation

T_h we will define the *computational domain* as

$$D_h := \left\{ x \in \Big(\bigcup_{K \in \mathcal{T}_h} \overline{K} \Big)^\circ \right\}$$

and will refer to its boundary $\Gamma_h := \partial D_h$ as the *computational boundary*. An example of the construction of D_h is shown in the left panel of Fig. 1.

We will say that e is an interior edge or face of the triangulation $\mathcal{T}_h$ if there are two elements K^+ and K^- in $\mathcal{T}_h$, such that, $e = \partial K^+ \cap \partial K^-$. In the same way, we will say that e is a boundary edge or face if there is an element $K \in \mathcal{T}_h$ such that $e = \partial K \cap \Gamma_h$. We will let $\mathcal{E}_h$ be the set of all edges or faces of the triangulation, $\mathcal{E}_h^\circ$ be the set of interior edges or faces, and $\mathcal{E}_h^\partial$ the set of exterior edges or faces of $\mathcal{T}_h$. Thus $\mathcal{E}_h = \mathcal{E}_h^\circ \cup \mathcal{E}_h^\partial$.

The outward unit normal of the element $K \in \mathcal{T}_h$ will be denoted by $\boldsymbol{n}$ and will denote it by $\boldsymbol{n}_e$ whenever we want to emphasize that $\boldsymbol{n}$ is the normal to a particular face e. Moreover, for each edge or face e of K, we denote the height of the element with respect to that edge or face as $h_e^\perp$. On a similar vein, for every boundary edge/face $e \in \partial\mathcal{E}_h$, we define $H_e^\perp$ as the length of the longest segment connecting e and Γ that is both parallel to the normal direction $\boldsymbol{n}_e$ and completely contained in K_{ext}^e. We then define the parameter

$$r_e := H_e^\perp / h_e^\perp ,$$

that serves as a measure of the local distance between Γ and Γ_h, relative to the local mesh size. Related to this, we have the *proximity parameter*

$$R := \max_{e \in \mathcal{E}_h^\partial} r_e .$$

Admissible triangulations

For all the analysis that follows, we will consider only families $\{\mathcal{T}_h\}_{h>0}$ of admissible triangulations, where a triangulation $\mathcal{T}_h$ is said to be *admissible* if the following conditions are satisfied:

1. There exists a constant $r > 0$ such that $rh \leq \underline{h}$. This condition is known as *quasi uniformity*.
2. There exists $\rho > 0$ such that, for any triangle $K \in \mathcal{T}_h$ we have that $\operatorname{diam}(B_K) \geq \rho \operatorname{diam}(K)$, where B_K is the biggest ball inscribed in the element K. This condition is called *uniform shape regularity*.
3. If for any two distinct elements $K, K' \in \mathcal{T}_h$ it holds that the intersection $K \cap K'$ is either empty, it consists of a single common vertex or a single common edge/face. When this holds we say that the triangulation has no *hanging nodes*. This is in fact not a necessary, but it considerably simplifies the analysis [6, 17, 18].
4. There exists a bijective function
$$\boldsymbol{\phi} : \Gamma_h \longrightarrow \Gamma \tag{12}$$
That, for every point $\boldsymbol{x} \in \Gamma_h$, assigns a point $\bar{\boldsymbol{x}} := \boldsymbol{\phi}(\boldsymbol{x}) \in \Gamma$ such that the straight segment connecting $\overline{\boldsymbol{x}}$ to $\boldsymbol{x}$ satisfies the following conditions:
   (a) Does not intersect the interior of the computational domain D_h.
   (b) $|\boldsymbol{x} - \bar{\boldsymbol{x}}| \leq Ch^{n+\delta}$, for some $C > 0$, $n \in \mathbb{N}$ and $0 < \delta < 1$. We refer to this as the *local proximity condition of order* n. For Dirichlet problems, it is enough to require $n = 1$ [53, 56]. This condition can also be expressed as
   $$\max_{e \in \mathcal{E}_h^\partial} H_e^\perp \leq Ch^{n+\delta} . \tag{13}$$
   (c) There exist generic positive constants such that
   $$\|\psi \boldsymbol{n} \circ \boldsymbol{\phi}\|_{\Gamma_h} \lesssim \|\psi \boldsymbol{n}\|_\Gamma \lesssim \|\psi \boldsymbol{n} \circ \boldsymbol{\phi}\|_{\Gamma_h} \tag{14}$$
   for every $\psi \in H^1(\Omega) \cap H^1(\Omega_h)$.

Up to this point, the conditions imposed on admissible triangulations have had a purely geometric character. They have pertained solely to the capability of a family of triangulations to smoothly approximate the desired domain as the mesh is refined. The next batch of conditions considers the interaction of the physical parameters, the geometry and a stabilization parameter characteristic of HDG. In particular, they will determine the maximum admissible

distance between the computational and physical boundaries in terms of the physical parameters, the stabilization parameter and the polynomial degree of the approximation.

We start by introducing the a pair of edge–wise constant functions that will be useful in the convergence analysis

$$C_e^{ext} := \frac{1}{\sqrt{r_e}} \sup_{\boldsymbol{\zeta}\in[\mathbb{P}_k(K^e)]^d\cdot\boldsymbol{n}_e\setminus\{\mathbf{0}\}} \frac{\|\boldsymbol{\zeta}\|_{K^e_{ext}}}{\|\boldsymbol{\zeta}\|_{K^e}}, \qquad \text{and} \qquad C_e^{inv} := h_e^{\perp} \sup_{\boldsymbol{\zeta}\in[\mathbb{P}_k(K^e)]^d\cdot\boldsymbol{n}_e\setminus\{\mathbf{0}\}} \frac{\|\partial_{\boldsymbol{n}_e}\boldsymbol{\zeta}\|_{K^e}}{\|\boldsymbol{\zeta}\|_{K^e}},$$

where $\mathbb{P}_k(D)$ denotes the set of polynomials of degree at most k over the domain D. As proven in [24], these functions can be bounded globally in terms of the polynomial degree of the approximation k and the mesh regularity parameter as

$$C_e^{ext} \leq C_1(k+1)^2(3\beta+2)^k \tag{15a}$$

$$C_e^{inv} \leq C_2 k^2 \tag{15b}$$

Finally, we introduce the mesh–dependent function $\tau : \mathcal{E}_h \to \mathbb{R}$, which will act as a stabilization parameter and will be used in the analysis of sections 4 and 5. In the most general case, this stabilization function needs only to be strictly positive and essentially bounded (i.e. $\tau \in L^\infty(\mathcal{E}_h)$). However, in this work we will consider it to be simply any positive constant.

With these definitions we are prepared to establish our next set of assumptions, which will be used from now on for the analysis in the following sections.

5. For every $e \in \mathcal{E}_h^\partial$, the maximum distance between Γ and Γ_h satisfies

$$H_e^{\perp} \leq \left(4\tau \cdot \min\left\{1, \max_{\boldsymbol{x}\in\Gamma_h}(1+a^{-1})\right\}\right)^{-1}. \tag{16}$$

   Regarding this somewhat esoteric condition we can state the following. Recalling that a^{-1} is the reciprocal of the diffusivity coefficient, it informs about the possible formation of boundary layers—which are likely to be present if a^{-1} is large. Therefore, the distance between the physical and computational boundaries must be aware about this value. On the other hand, the stabilization parameter τ penalizes the size of the jump of the discrete approximations across adjacent elements. A large value of τ will reduce the size of the jump and will make it more difficult to approximate a steep gradient (or a boundary layer) across an element. If this is the case, the distance between boundaries must be reduced.

6. The local proximity parameter must satisfy

$$R < 2^{-1/3}\left(C_e^{inv}C_e^{ext}\right)^{-2/3}. \tag{17}$$

   In view of the estimates (15) and the fact that—as we will soon explain in detail—we will extrapolate some approximations from Γ_h to Γ, this estimate sets an acceptable ratio in terms of the polynomial degree of the approximation.

Transfer paths

We must now describe how to transfer the boundary data from the problem boundary Γ to the computational boundary Γ_h. We will refer to the straight segment from condition 4 above as a *transfer path* associated to $\boldsymbol{x}$. We will denote its unit tangent vector and its length respectively by

$$\boldsymbol{t}(\boldsymbol{x}) := (\boldsymbol{x}-\overline{\boldsymbol{x}})/|\boldsymbol{x}-\overline{\boldsymbol{x}}|, \qquad \text{and} \qquad l(\boldsymbol{x}) := |\boldsymbol{x}-\overline{\boldsymbol{x}}|.$$

This construction is represented schematically in the center–left panel of Fig. 1.

Since $\boldsymbol{\phi}$ is a bijection, each boundary face $e \in \partial\mathcal{E}_h$ will be identified with its corresponding image in Γ, which we will denote by

$$\Gamma_e := \{\overline{\boldsymbol{x}} \in \Gamma : \overline{\boldsymbol{x}} = \boldsymbol{\phi}(\boldsymbol{x}) \quad \text{for some} \quad \boldsymbol{x} \in e\}.$$

A depiction of the segment Γ_e associated to an edge e is shown in the center right panel of Fig. 1. An algorithm for constructing a collection of transfer paths, satisfying the additional condition that no transfer paths do not intersect each other, was developed in [24] for the two dimensional case. The intersection–avoiding condition is not necessary for the analysis, but provides a simple and natural way to construct the extension patches that will be defined below.

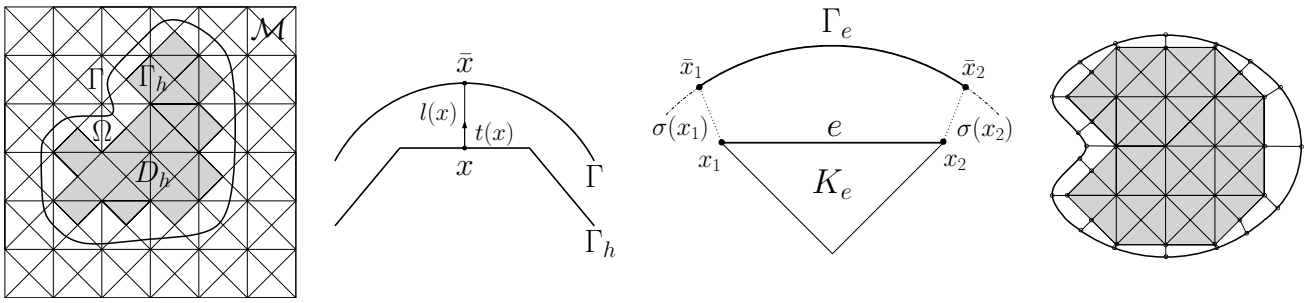

Figure 1: Left: Example of a domain Ω, its boundary Γ, a background domain $\mathcal{M}$ and the construction of the computational domain D_h, shaded in gray. Center left: A transfer path associated to $\boldsymbol{x}$. Center right: The extension patch K_e^{ext} is the region enclosed by the edge e, the segment Γ_e and the transfer paths $\sigma(\boldsymbol{x}_1)$ and $\sigma(\boldsymbol{x}_2)$. Right: Tessellation of the full domain. The extension patches are the white tiles filling the space between Γ and Γ_h.

Extension patches

For computational purposes that will become clear soon, we will have to tessellate the complement of the computational domain $D_h^c := \Omega \backslash \overline{D_h}$ in such a way that there is a one-to one correspondence between boundary edges $e \in \mathcal{E}_h^\partial$ and tiles in the tessellation. We will denote by K_e^{ext} the only tile that has e as a face and will refer to it as an *extension patch*. One possible way of constructing such a tessellation is to use the algorithm from [24] and define the extension patch K_e^{ext} as the region bounded by the edge e, the transfer paths associated to the endpoints of e and the segment of Γ delimited by the transfer paths, as depicted in the two panels on the right of (1).

If K_e is the element that shares the edge e with the extension patch K_e^{ext} and p is a polynomial defined over K_e, we define the extrapolation of p from K_e to K_e^{ext} by

$$E_h(p)(y) := p(y) \quad \text{for all} \quad y \in K_e^{ext}.$$

To simplify notation, whenever possible we will simply notation by simply writing $p(y)$ understanding that the extrapolation operator is used tacitly.

4 Unfitted HDG discretizations

In this section we present and analyze HDG schemes for the state, adjoint and deformation field equations—the latter inspired by [49]. All the schemes will make use of the transfer path technique [29, 24] introduced in the previous section. This will allow us to pose the HDG discretization using only polyhedral elements, even in domains which are not necessarily polyhedral.

The discretization will use the following global polynomial spaces:

$$\boldsymbol{Z}_h := \left\{ \boldsymbol{v} \in [L^2(\mathcal{T}_h)]^d \,:\, \boldsymbol{v}|_K \in [\mathbb{P}_k(K)]^d \quad \forall\, K \in \mathcal{T}_h \right\}, \tag{18a}$$

$$W_h := \left\{ w \in L^2(\mathcal{T}_h) \,:\, w|_K \in \mathbb{P}_k(K) \quad \forall\, K \in \mathcal{T}_h \right\}, \tag{18b}$$

$$M_h := \left\{ \mu \in L^2(\mathcal{E}_h) \,:\, \mu|_e \in \mathbb{P}_k(e) \quad \forall\, e \in \mathcal{E}_h \right\}. \tag{18c}$$

We will also use the following inner products associated to $\mathcal{T}_h$ and $\partial\mathcal{T}_h$

$$(u,v)_{D_h} := \sum_{K\in\mathcal{T}_h} \int_K u\, v \qquad \text{and} \qquad \langle s,t\rangle_{\mathcal{E}_h} := \sum_{K\in\mathcal{T}_h} \int_{\partial K} s\, t\,,$$

which induce the norms

$$\|u\|_{D_h} := (u,u)_{D_h}^{1/2} \qquad \text{and} \qquad \|s\|_{\mathcal{E}_h} := \langle s,s\rangle_{\mathcal{E}_h}^{1/2}.$$

If w is a positive function defined along every edge of the triangulation, we define the weighted norms

$$\|v\|_{\mathcal{E}_h,w} := \|w^{1/2}v\|_{\mathcal{E}_h} \qquad \text{and} \qquad \|v\|_{\Gamma,w} := \left(\sum_{e\subset\Gamma_h} \int_e w\,|v|^2 \right)^{1/2}. \tag{19}$$

The same notation will be used for tensor- and vector-valued polynomial functions defined on K^e.

State and adjoint equations

As proposed in [24], we consider the strong mixed formulations for the state and adjoint equations, restricted to the polygonal domain D_h:

$$
\begin{aligned}
a^{-1}\,\boldsymbol{p} + \nabla y &= 0 && \text{in } D_h\,, && \text{(20a)}\\
\nabla\cdot\boldsymbol{p} &= f && \text{in } D_h\,, && \text{(20b)}\\
y &= \varphi_1 && \text{on } \Gamma_h\,, && \text{(20c)}
\end{aligned}
\qquad\qquad
\begin{aligned}
a^{-1}\,\boldsymbol{r} + \nabla z &= 0 && \text{in } D_h\,, && \text{(21a)}\\
\nabla\cdot\boldsymbol{r} - y &= -\widetilde{y} && \text{in } D_h\,, && \text{(21b)}\\
z &= \varphi_2 && \text{on } \Gamma_h\,, && \text{(21c)}
\end{aligned}
$$

where the unknowns φ_1 and φ_2 correspond to the traces of y and z, respectively, on Γ_h. Let $\boldsymbol{x}\in\Gamma_h$ and $\bar{\boldsymbol{x}}$ its corresponding point on Γ. By integrating (20a) and (21a) along the transfer path joining $\boldsymbol{x}$ and $\bar{\boldsymbol{x}}$, we obtain

$$
\varphi_1(\boldsymbol{x}) := g(\bar{\boldsymbol{x}}) + \int_0^{l(\boldsymbol{x})} a^{-1}\,\boldsymbol{p}\,(\boldsymbol{x}+s\,\boldsymbol{t})\cdot\boldsymbol{t}\,ds \qquad\text{and}\qquad \varphi_2(\boldsymbol{x}) := \int_0^{l(\boldsymbol{x})} a^{-1}\,\boldsymbol{r}\,(\boldsymbol{x}+s\,\boldsymbol{t})\cdot\boldsymbol{t}\,ds\,. \tag{22}
$$

The HDG method for the state equation seeks an approximation $(\boldsymbol{p}_h, y_h, \widehat{y}_h)$ of the exact solution $(\boldsymbol{p}, y, y|_{\mathcal{E}_h})$ in the space $\boldsymbol{Z}_h\times W_h\times M_h$ satisfying

$$
\begin{aligned}
(a^{-1}\,\boldsymbol{p}_h,\boldsymbol{v}_1)_{D_h} - (y_h,\nabla\cdot\boldsymbol{v}_1)_{D_h} + \langle\widehat{y}_h,\boldsymbol{v}_1\cdot\boldsymbol{n}_h\rangle_{\mathcal{E}_h} &= 0\,, && \text{(23a)}\\
-(\boldsymbol{p}_h,\nabla w_1)_{D_h} + \langle\widehat{\boldsymbol{p}}_h\cdot\boldsymbol{n}_h, w_1\rangle_{\mathcal{E}_h} &= (f,w_1)_{D_h}\,, && \text{(23b)}\\
\langle\widehat{\boldsymbol{p}}_h\cdot\boldsymbol{n}_h,\mu_1\rangle_{\mathcal{E}_h\setminus\Gamma_h} &= 0\,, && \text{(23c)}\\
\langle\widehat{y}_h,\mu_1\rangle_{\Gamma_h} &= \langle\varphi_1^h,\mu_1\rangle_{\Gamma_h}\,, && \text{(23d)}
\end{aligned}
$$

for all $(\boldsymbol{v}_1, w_1, \mu_1)\in\boldsymbol{Z}_h\times W_h\times M_h$. In turn, the HDG method for the adjoint equation seeks and approximation $(\boldsymbol{r}_h, z_h, \widehat{z}_h)$ of the exact solution $(\boldsymbol{r}, z, z|_{\mathcal{E}_h})$ in the space $\boldsymbol{Z}_h\times W_h\times M_h$ such that

$$
\begin{aligned}
(a^{-1}\,\boldsymbol{r}_h,\boldsymbol{v}_2)_{D_h} - (z_h,\nabla\cdot\boldsymbol{v}_2)_{D_h} + \langle\widehat{z}_h,\boldsymbol{v}_2\cdot\boldsymbol{n}\rangle_{\mathcal{E}_h} &= 0\,, && \text{(24a)}\\
-(\boldsymbol{r}_h,\nabla w_2)_{D_h} + \langle\widehat{\boldsymbol{r}}_h\cdot\boldsymbol{n}_h, w_2\rangle_{\mathcal{E}_h} &= (y_h-\widetilde{y},w_2)_{D_h}\,, && \text{(24b)}\\
\langle\widehat{\boldsymbol{r}}_h\cdot\boldsymbol{n}_h,\mu_2\rangle_{\mathcal{E}_h\setminus\Gamma_h} &= 0\,, && \text{(24c)}\\
\langle\widehat{z}_h,\mu_2\rangle_{\Gamma_h} &= \langle\varphi_2^h,\mu_2\rangle_{\Gamma_h}\,, && \text{(24d)}
\end{aligned}
$$

for all $(\boldsymbol{v}_2, w_2, \mu_2)\in\boldsymbol{Z}_h\times W_h\times M_h$. The functions φ_1^h and φ_2^h appearing in the systems above are discrete analogs of (22). They transfer the Dirichlet boundary conditions from Γ to Γ_h and are defined along all faces in $\mathcal{E}_h^\partial$, by

$$
\begin{aligned}
\varphi_1^h(\boldsymbol{x}) &:= g(\bar{\boldsymbol{x}}) + \int_0^{l(\boldsymbol{x})} a^{-1}\,E_h(\boldsymbol{p}_h)(\boldsymbol{x}+s\,\boldsymbol{t}(\boldsymbol{x}))\cdot\boldsymbol{t}(\boldsymbol{x})\,ds\,,\\
\varphi_2^h(\boldsymbol{x}) &:= \int_0^{l(\boldsymbol{x})} a^{-1}\,E_h(\boldsymbol{r}_h)(\boldsymbol{x}+s\,\boldsymbol{t}(\boldsymbol{x}))\cdot\boldsymbol{t}(\boldsymbol{x})\,ds\,,
\end{aligned}
\tag{25}
$$

where $E_h(\boldsymbol{p}_h)$ and $E_h(\boldsymbol{r}_h)$ are the extrapolation of $\boldsymbol{p}_h$ and $\boldsymbol{r}_h$ respectively. The numerical fluxes $\widehat{\boldsymbol{p}}_h$ and $\widehat{\boldsymbol{r}}_h$ are defined along every edge $e\in\mathcal{E}_h$ by

$$
\widehat{\boldsymbol{p}}_h = \boldsymbol{p}_h + \tau\,(y_h-\widehat{y}_h)\,\boldsymbol{n}_h \qquad\text{and}\qquad \widehat{\boldsymbol{r}}_h = \boldsymbol{r}_h + \tau\,(z_h-\widehat{z}_h)\,\boldsymbol{n}_h\,, \tag{26}
$$

and τ is a positive and bounded stabilization function defined on $\mathcal{E}_h$, whose maximum and minimum values will be denoted respectively by $\overline{\tau}$ and $\underline{\tau}$.

The unfitted schemes in (23) and (24) were studied in [24], where their well-posedness was established. We will use this result without not repeating the argument here. Instead we will now move on to study the discretization of the deformation field.

The deformation field equation

We now present the HDG scheme for the deformation field equation which is inspired by the work done on [49]. It shall be noted that, due to the presence of a Neumann boundary condition, the treatment cannot be the same as in the cases of the state and adjoint equations. In particular, a transfer function in the style of (22) to transfer the Neumann data from the curved boundary Γ to the polygonal computational boundary Γ_h is not available.

Instead, we will make use of the bijection $\boldsymbol{\phi}$ defined on (12) to impose the Neumann condition on the computational boundary. Under these conditions, the deformation field equation can be written in the computational domain D_h as follows:

$$\boldsymbol{\sigma} + \nabla \boldsymbol{V} = 0 \qquad \text{in } D_h\,, \tag{27a}$$
$$\mathbf{div}(\boldsymbol{\sigma}) = \mathbf{0} \qquad \text{in } D_h\,, \tag{27b}$$
$$\boldsymbol{\sigma}\,\boldsymbol{n}_h = \boldsymbol{g}_N \quad \text{on } \Gamma_h^N\,, \tag{27c}$$
$$\boldsymbol{V} = \boldsymbol{g}_D \quad \text{on } \Gamma_h^D\,. \tag{27d}$$

We assume that the computational boundary Γ_h is split between Γ_h^D (the part of Γ_h with Dirichlet datum) and Γ_h^N (the part of Γ_h with Neumann datum) in such a way that

$$\Gamma_h = \Gamma_h^D \cup \Gamma_h^N \qquad \text{and} \qquad \Gamma_h^D \cap \Gamma_h^N = \varnothing.$$

The Neumann datum $\boldsymbol{g}_N$ is defined by

$$\boldsymbol{g}_N := (G(\Gamma)\boldsymbol{n}) \circ \boldsymbol{\phi}\,,$$

Where $G(\Gamma)$ is as defined in (4), and the transfer function $\boldsymbol{\phi}$ is the one defined on (12). Recalling the mixed variables

$$\nabla y = -\,a^{-1}\,\boldsymbol{p} \qquad \text{and} \qquad \nabla z = -\,a^{-1}\,\boldsymbol{r}$$

introduced in the state and adjoint mixed formulations, we can rewrite $G(\Gamma)$ as

$$G(\Gamma) = \boldsymbol{r}\cdot\boldsymbol{n}(a^{-1}\,\boldsymbol{p}\cdot\boldsymbol{n} + \partial_{\boldsymbol{n}} g) + \frac{1}{2}(g - \widetilde{y})^2\,. \tag{28}$$

The Dirichlet datum $\boldsymbol{g}_D$ is transferred using the same technique used in the state and adjoint equations, that is,

$$\boldsymbol{g}_D(\boldsymbol{x}) := \int_0^{l(\boldsymbol{x})} \boldsymbol{\sigma}(\boldsymbol{x} + s\,\boldsymbol{t})\,\boldsymbol{t}\,ds\,.$$

Before presenting the discrete scheme, we define the vector–valued polynomial spaces used for the discretization, which are defined as

$$\begin{aligned}
\mathbb{Z}_h &:= \{\boldsymbol{\xi} \in [L^2(\mathcal{T}_h)]^{d\times d} \,:\, \boldsymbol{\xi}|_K \in [\mathbb{P}_k(K)]^{d\times d}\,, \quad \forall\, K \in \mathcal{T}_h\}\,,\\
\boldsymbol{W}_h &:= \{\boldsymbol{w} \in [L^2(\mathcal{T}_h)]^{d} \,:\, \boldsymbol{w}|_K \in [\mathbb{P}_k(K)]^{d}\,, \quad \forall\, K \in \mathcal{T}_h\}\,,\\
\boldsymbol{M}_h &:= \{\boldsymbol{\mu} \in [L^2(\mathcal{E}_h)]^{d} \,:\, \boldsymbol{\mu}|_e \in [\mathbb{P}_k(e)]^{d}\,, \quad \forall\, e \in \mathcal{E}_h\}\,.
\end{aligned}$$

Then, our discrete scheme seeks an approximation $(\boldsymbol{\sigma}_h, \boldsymbol{V}_h, \widehat{\boldsymbol{V}}_h) \in \mathbb{Z}_h \times \boldsymbol{W}_h \times \boldsymbol{M}_h$ of the exact solution $(\boldsymbol{\sigma}, \boldsymbol{V}_h, \boldsymbol{V}_h|_{\mathcal{E}_h})$, which is given by

$$(\boldsymbol{\sigma}_h, \boldsymbol{\psi})_{D_h} - (\boldsymbol{V}_h, \mathbf{div}(\boldsymbol{\psi}))_{D_h} + \langle \widehat{\boldsymbol{V}}_h, \boldsymbol{\psi}\,\boldsymbol{n}_h\rangle_{\mathcal{E}_h} = 0\,, \tag{30a}$$
$$-(\boldsymbol{\sigma}_h, \nabla \boldsymbol{w})_{D_h} + \langle \widehat{\boldsymbol{\sigma}}_h\,\boldsymbol{n}_h, \boldsymbol{w}\rangle_{\mathcal{E}_h} = 0\,, \tag{30b}$$
$$\langle \widehat{\boldsymbol{\sigma}}_h\,\boldsymbol{n}_h, \boldsymbol{\mu}\rangle_{\mathcal{E}_h\setminus\Gamma_h} = 0\,, \tag{30c}$$
$$\langle \widehat{\boldsymbol{\sigma}}_h\,\boldsymbol{n}_h, \boldsymbol{\mu}\rangle_{\Gamma_h^N} = \langle (G_h(\Gamma)\boldsymbol{n}) \circ \boldsymbol{\phi}, \boldsymbol{\mu}\rangle_{\Gamma_h^N}\,, \tag{30d}$$
$$\langle \widehat{\boldsymbol{V}}_h, \boldsymbol{\mu}\rangle_{\Gamma_h^D} = \langle \boldsymbol{g}_h^D, \boldsymbol{\mu}\rangle_{\Gamma_h^D}\,, \tag{30e}$$

for all $(\boldsymbol{\psi}, \boldsymbol{w}, \boldsymbol{\mu}) \in \mathbb{Z}_h \times \boldsymbol{W}_h \times \boldsymbol{M}_h$, where

$$\widehat{\boldsymbol{\sigma}}_h\,\boldsymbol{n}_h := \boldsymbol{\sigma}_h\,\boldsymbol{n}_h + \tau\,(\boldsymbol{V}_h - \widehat{\boldsymbol{V}}_h)\,, \tag{30f}$$
$$G_h(\Gamma) := \boldsymbol{r}_h\cdot\boldsymbol{n}\,(a^{-1}\,\boldsymbol{p}_h\cdot\boldsymbol{n} + \partial_{\boldsymbol{n}} g) + \frac{1}{2}(g - \widetilde{y})^2\,, \tag{30g}$$
$$\boldsymbol{g}_h^D(\boldsymbol{x}) := \int_0^{l(\boldsymbol{x})} E_h(\boldsymbol{\sigma}_h)(\boldsymbol{x} + s\,\boldsymbol{t}(\boldsymbol{x}))\,\boldsymbol{t}(\boldsymbol{x})\,ds\,. \tag{30h}$$

From now on, for the sake of simplicity, we assume $\boldsymbol{t}(\boldsymbol{x}) = \boldsymbol{n}_h$ for all $\boldsymbol{x} \in e$ and all $e \subset \Gamma_h^D$. Otherwise, the results follow from assuming $\boldsymbol{t}\cdot\boldsymbol{n}_h > 0$ and analyzing the tangential and normal components separately.

Theorem 4.1. *If $\mathcal{T}_h$ is a sufficiently fine admissible triangulation, then there exists a unique solution of the HDG scheme (30) associated to the deformation field equation.*

Proof. We will use the Fredholm alternative. Let us start by assuming that $G_h(\Gamma) = 0$ and by taking test functions

$$\boldsymbol{\psi} = \boldsymbol{\sigma}_h\,, \qquad \boldsymbol{w} = \boldsymbol{V}_h\,, \quad \text{and} \quad \boldsymbol{\mu} = \begin{cases} \widehat{\boldsymbol{V}}_h \ \text{ in } \ \mathcal{E}_h \setminus \Gamma_h^D \\ \widehat{\boldsymbol{\sigma}}_h \boldsymbol{n}_h \ \text{ in } \ \Gamma_h^D \end{cases}.$$

Substituting the chosen value of $\boldsymbol{\mu}$ into (30c), (30e), and (30d), and adding the resulting expressions shows that

$$\langle \widehat{\boldsymbol{\sigma}}_h\, \boldsymbol{n}_h, \widehat{\boldsymbol{V}}_h \rangle_{\mathcal{E}_h} \;=\; \langle \widehat{\boldsymbol{\sigma}}_h\, \boldsymbol{n}_h, \boldsymbol{g}_h^D \rangle_{\Gamma_h^D}. \tag{31}$$

Then, integrating by parts (30b) and adding the resulting expression to (30a), we get

$$\begin{aligned} 0 &= \|\boldsymbol{\sigma}_h\|_{D_h}^2 \;+\; \langle (\widehat{\boldsymbol{\sigma}}_h - \boldsymbol{\sigma}_h)\boldsymbol{n}_h, \boldsymbol{V}_h \rangle_{\mathcal{E}_h} \;+\; \langle \boldsymbol{\sigma}_h\, \boldsymbol{n}_h, \widehat{\boldsymbol{V}}_h \rangle_{\mathcal{E}_h} \\ &= \|\boldsymbol{\sigma}_h\|_{D_h}^2 \;+\; \|\tau^{1/2}\,(\boldsymbol{V}_h - \widehat{\boldsymbol{V}}_h)\|_{\mathcal{E}_h}^2 \;+\; \langle \widehat{\boldsymbol{\sigma}}_h\, \boldsymbol{n}_h, \widehat{\boldsymbol{V}}_h \rangle_{\mathcal{E}_h} \qquad \text{(Using (30f))} \\ &= \|\boldsymbol{\sigma}_h\|_{D_h}^2 \;+\; \|\tau^{1/2}\,(\boldsymbol{V}_h - \widehat{\boldsymbol{V}}_h)\|_{\mathcal{E}_h}^2 \;+\; \langle \widehat{\boldsymbol{\sigma}}_h\, \boldsymbol{n}_h, \boldsymbol{g}_h^D \rangle_{\Gamma_h^D} \qquad \text{(By (31))}. \end{aligned} \tag{32}$$

On the other hand, adding and subtracting $\boldsymbol{\sigma}_h$ in the definition of $\boldsymbol{g}_h^D$, we can write

$$\boldsymbol{g}_h^D(\boldsymbol{x}) \;=\; \int_0^{l(\boldsymbol{x})} (E_h(\boldsymbol{\sigma}_h)(\boldsymbol{x} \,+\, s\,\boldsymbol{n}_h) \,-\, \boldsymbol{\sigma}_h(\boldsymbol{x}))\cdot \boldsymbol{n}_h\, ds \,+\, \boldsymbol{\sigma}_h(\boldsymbol{x})\,\boldsymbol{n}_h\, l(\boldsymbol{x})\,,$$

which leads to the expression

$$\boldsymbol{\sigma}_h(\boldsymbol{x})\,\boldsymbol{n}_h \;=\; l^{-1}(\boldsymbol{x})\,\boldsymbol{g}_h^D(\boldsymbol{x}) \,-\, \Lambda^{\boldsymbol{\sigma}_h}(\boldsymbol{x}),$$

where, to keep notation compact, we have defined the term

$$\Lambda^{\boldsymbol{\sigma}_h}(\boldsymbol{x}) := \frac{1}{l(\boldsymbol{x})} \int_0^{l(\boldsymbol{x})} (\boldsymbol{E}(\boldsymbol{\sigma}_h)(\boldsymbol{x} \,+\, s\,\boldsymbol{n}_h) \,-\, \boldsymbol{\sigma}_h(\boldsymbol{x}))\cdot \boldsymbol{n}_h\, ds\,. \tag{33}$$

Then,substituting the expression for $\boldsymbol{\sigma}_h(\boldsymbol{x})\,\boldsymbol{n}_h$ obtained above into (30f), we have that

$$\langle \widehat{\boldsymbol{\sigma}}_h\, \boldsymbol{n}_h, \boldsymbol{g}_h^D \rangle_{\Gamma_h^D} \;=\; \|l^{-1/2}\,\boldsymbol{g}_h^D\|_{\Gamma_h^D}^2 + \langle l^{1/2}(\tau\,(\boldsymbol{V}_h - \widehat{\boldsymbol{V}}_h) - \Lambda^{\boldsymbol{\sigma}_h}), l^{-1/2}\,\boldsymbol{g}_h^D \rangle_{\Gamma_h^D}\,.$$

Substituting this into (32) we find that

$$\|\boldsymbol{\sigma}_h\|_{D_h}^2 \;+\; \|\tau^{1/2}\,(\boldsymbol{V}_h - \widehat{\boldsymbol{V}}_h)\|_{\mathcal{E}_h}^2 \;+\; \|l^{-1/2}\,\boldsymbol{g}_h^D\|_{\Gamma_h^D}^2 \;=\; \langle l^{1/2}(\Lambda^{\boldsymbol{\sigma}_h} - \tau\,(\boldsymbol{V}_h - \widehat{\boldsymbol{V}}_h)), l^{-1/2}\,\boldsymbol{g}_h^D \rangle_{\Gamma_h^D}\,.$$

Now, we use Young's inequality to bound the right-hand side of the expression above as

$$\begin{aligned} \langle l^{1/2}(\Lambda^{\boldsymbol{\sigma}_h} - \tau\,(\boldsymbol{V}_h - \widehat{\boldsymbol{V}}_h)), l^{-1/2}\,\boldsymbol{g}_h^D \rangle_{\Gamma_h^D} &\le \tfrac{1}{2}\left(\|l^{1/2}\Lambda^{\boldsymbol{\sigma}_h}\|_{\Gamma_h^D}^2 + \|l^{1/2}\tau(\boldsymbol{V}_h - \widehat{\boldsymbol{V}}_h)\|_{\Gamma_h^D}^2 + \|l^{-1/2}\boldsymbol{g}_h^D\|_{\Gamma_h^D}^2 \right) \\ &\le \tfrac{1}{2}\left(H_e^{\perp}\|\Lambda^{\boldsymbol{\sigma}_h}\|_{\Gamma_h^D}^2 + H_e^{\perp}\|\tau(\boldsymbol{V}_h - \widehat{\boldsymbol{V}}_h)\|_{\Gamma_h^D}^2 + \|l^{-1/2}\boldsymbol{g}_h^D\|_{\Gamma_h^D}^2 \right). \end{aligned}$$

From the last two expressions it follows that

$$\begin{aligned} \|\boldsymbol{\sigma}_h\|_{D_h}^2 + (1 - \tfrac{1}{2}H_e^{\perp})\left(\|\tau^{1/2}(\boldsymbol{V}_h - \widehat{\boldsymbol{V}}_h)\|_{\mathcal{E}_h}^2 + \|l^{-1/2}\,\boldsymbol{g}_h^D\|_{\Gamma_h^D}^2 \right) &\le \tfrac{1}{2}H_e^{\perp}\|\Lambda^{\boldsymbol{\sigma}_h}\|_{\Gamma_h^D}^2 \\ &\le \tfrac{1}{6}H_e^{\perp} r_e^3 (C_e^{ext} C_e^{inv})^2 \|\boldsymbol{\sigma}_h\|_{D_h}^2 \qquad \text{(By (56))} \\ &\le \tfrac{1}{2}H_e^{\perp}\|\boldsymbol{\sigma}_h\|_{D_h}^2 \qquad \text{(By (17))}. \end{aligned}$$

Hence, the local proximity condition (13) implies that if the mesh is sufficiently fine

$$\boldsymbol{\sigma}_h = \boldsymbol{0} \qquad \text{in } D_h\,, \tag{34a}$$

$$\boldsymbol{V}_h = \widehat{\boldsymbol{V}}_h \qquad \text{on } \mathcal{E}_h\,, \tag{34b}$$

$$\boldsymbol{g}_h^D = \boldsymbol{0} \qquad \text{on } \Gamma_h^D. \tag{34c}$$

From here, we see that integrating by parts the second term in equation (30a), letting $\boldsymbol{\psi} = \nabla \boldsymbol{V}_h$, and using (34a), it follows that $\|\nabla \boldsymbol{V}_h\|_{D_h} = 0$. On the other hand, (34b) and (34c) together with (30e) imply

$$\langle \boldsymbol{V}_h, \boldsymbol{\mu} \rangle_{\Gamma_h^D} = \langle \widehat{\boldsymbol{V}}_h, \boldsymbol{\mu} \rangle_{\Gamma_h^D} = \langle \boldsymbol{g}_h^D, \boldsymbol{\mu} \rangle_{\Gamma_h^D} = 0$$

for all $\mu \in \boldsymbol{M}_h$. Hence, $\boldsymbol{V}_h = 0$ in D_h. Since the only solution to the homogeneous problem is the trivial one, the problem is uniquely solvable by the Fredholm alternative. □ □

5 *A priori* error estimates.

For the error analysis we will make use of the HDG projection introduced in [22] and summarized in the Appendix B for convenience. For a discrete space X_h we will denote its HDG projector by Π_X and the L^2 projector by P_X and use them to define the projections of the error for all our unknowns:

$$\begin{aligned}
&\boldsymbol{\varepsilon_p} := \boldsymbol{\Pi_Z p} - \boldsymbol{p}_h\,, && \varepsilon_y := \Pi_W y - y_h\,, && \varepsilon_{\widehat{y}} := P_M y - \widehat{y}_h\,, && \boldsymbol{\varepsilon_{\widehat{p}}} := P_M \boldsymbol{p} - \widehat{\boldsymbol{p}}_h\,, && \text{(State)}\\
&\boldsymbol{\varepsilon_r} := \boldsymbol{\Pi_Z r} - \boldsymbol{r}_h\,, && \varepsilon_z := \Pi_W z - z_h\,, && \varepsilon_{\widehat{z}} := P_M z - \widehat{z}_h\,, && \boldsymbol{\varepsilon_{\widehat{r}}} := P_M \boldsymbol{r} - \widehat{\boldsymbol{r}}_h\,, && \text{(Adjoint)}\\
&\boldsymbol{\varepsilon_\sigma} := \boldsymbol{\Pi_{\mathbb{Z}} \sigma} - \boldsymbol{\sigma}_h\,, && \boldsymbol{\varepsilon_V} := \boldsymbol{\Pi_W V} - \boldsymbol{V}_h\,, && \varepsilon_{\widehat{\boldsymbol{V}}} := P_{\boldsymbol{M}} \boldsymbol{V} - \widehat{\boldsymbol{V}}_h\,, && \boldsymbol{\varepsilon_{\widehat{\sigma}}} := P_{\boldsymbol{M}} \boldsymbol{\sigma} - \widehat{\boldsymbol{\sigma}}_h\,, && \text{(Deformation)}
\end{aligned}$$

We also define the interpolation errors as

$$\begin{aligned}
I_{\boldsymbol{p}} &:= \boldsymbol{p} - \boldsymbol{\Pi_Z p}\,, & I_{\boldsymbol{r}} &:= \boldsymbol{r} - \boldsymbol{\Pi_Z r}\,, & \boldsymbol{I_\sigma} &:= \boldsymbol{\sigma} - \boldsymbol{\Pi_{\mathbb{Z}} \sigma}\,,\\
I_y &:= y - \Pi_W y\,, & I_z &:= z - \Pi_W z\,, & \boldsymbol{I_V} &:= \boldsymbol{V} - \boldsymbol{\Pi_W V}\,.
\end{aligned}$$

5.1 Error estimates for the state and adjoint equations

As mentioned before, the analysis for unfitted HDG schemes for independent equations of the type satisfied by the state and adjoint variables were analyzed in [24]. The main difference is that, for the present case, the problems are coupled through the adjoint boundary condition (21b). This is reflected in the presence of both variables in some of the error estimates below. Nevertheless, the results from [24] carry over in almost straightforward manner and we shall not repeat the arguments here. Instead, we summarize the error estimates in the following theorem.

Theorem 5.1 ([24] Theorem 2.1)**.** *Let $(y, \boldsymbol{p})$ be a solution pair to the state problem (20) and $(z, \boldsymbol{r})$ be a solution pair to the adjoint problem (21), and $(y_h, \boldsymbol{p}_h)$ and $(z_h, \boldsymbol{r}_h)$ be solutions to the corresponding HDG schemes (23) and (23). We have that*

$$\begin{aligned}
\|\boldsymbol{p} - \boldsymbol{p}_h\|_\Omega &\lesssim \|I_{\boldsymbol{p}}\|_{D_h} + \|I_{\boldsymbol{p}} \cdot \boldsymbol{n}\|_{\Gamma_h, h^\perp} + h^{k+1} |\boldsymbol{p}|_{\boldsymbol{H}^{k+1}(\Omega)}\,,\\
\|\boldsymbol{r} - \boldsymbol{r}_h\|_\Omega &\lesssim \|I_{\boldsymbol{r}}\|_{D_h} + \|I_{\boldsymbol{r}} \cdot \boldsymbol{n}\|_{\Gamma_h, h^\perp} + h^{k+1} |\boldsymbol{r}|_{\boldsymbol{H}^{k+1}(\Omega)} + \|\varepsilon_h^y\|_{D_h} + \|I_y\|_{D_h}.
\end{aligned}$$

Moreover, recalling the definition of the proximity parameter $R := \max_{e \in \mathcal{E}_h^\partial} r_e$ and

$$H_1 := \left(h + \tau^{1/2} R h + R^2 h^{1/2}\right), \qquad H_2 := \left(1 + \tau^{1/2} R h^{1/2}\right), \qquad H_3 := \left(h + R^{1/2} h + R^{3/2}\, h^{1/2}\right),$$

then the following estimate holds

$$\begin{aligned}
\|y - y_h\|_\Omega + \|z - z_h\|_\Omega \lesssim\; & H_1 \left(\|I_{\boldsymbol{p}}\|_{D_h} + \|I_{\boldsymbol{r}}\|_{D_h}\right) + R^{1/2} h \left(\|I_{\boldsymbol{p}} \cdot \boldsymbol{n}\|_{\Gamma_h, h^\perp} + \|I_{\boldsymbol{r}} \cdot \boldsymbol{n}\|_{\Gamma_h, h^\perp}\right)\\
& + H_2 \left(\|I_y\|_{D_h} + \|I_z\|_{D_h}\right) + H_3\, h^{k+1} \left(|\boldsymbol{p}|_{\boldsymbol{H}^{k+1}(\Omega)} + |\boldsymbol{r}|_{\boldsymbol{H}^{k+1}(\Omega)}\right).
\end{aligned}$$

Corollary 5.1.1. *If the stabilization parameter $\tau = \mathcal{O}(1)$, then,*

$$\|\boldsymbol{p} - \boldsymbol{p}_h\|_\Omega \lesssim h^{k+1}, \qquad \|y - y_h\|_\Omega \lesssim h^{k+1}, \qquad \|\boldsymbol{r} - \boldsymbol{r}_h\|_\Omega \lesssim h^{k+1}, \qquad \|z - z_h\|_\Omega \lesssim h^{k+1}.$$

5.2 Error estimates for $\boldsymbol{\sigma} - \boldsymbol{\sigma}_h$

We start by recalling that $\boldsymbol{n}_h$ to denotes the unitary normal vector for Γ_h, while $\boldsymbol{n}$ denotes the unitary normal vector for Γ. To begin with the analysis of the error for the velocity field equation, we note that the projections of

the errors satisfy the following equations

$$
\begin{aligned}
(\boldsymbol{\varepsilon}_{\boldsymbol{\sigma}}, \boldsymbol{\psi})_{D_h} - (\boldsymbol{\varepsilon}_{\boldsymbol{V}}, \mathbf{div}(\boldsymbol{\psi}))_{D_h} + \langle \boldsymbol{\varepsilon}_{\widehat{\boldsymbol{V}}}, \boldsymbol{\psi}\boldsymbol{n}_h\rangle_{\mathcal{E}_h} &= -(\boldsymbol{I}_{\boldsymbol{\sigma}}, \boldsymbol{\psi})_{D_h}\,, && \text{(35a)}\\
(\boldsymbol{\varepsilon}_{\boldsymbol{\sigma}}, \nabla \boldsymbol{w})_{D_h} - \langle \boldsymbol{\varepsilon}_{\widehat{\boldsymbol{\sigma}}}\boldsymbol{n}_h, \boldsymbol{w}\rangle_{\mathcal{E}_h} &= 0\,, && \text{(35b)}\\
\langle \boldsymbol{\varepsilon}_{\widehat{\boldsymbol{\sigma}}}\boldsymbol{n}_h, \boldsymbol{\mu}\rangle_{\mathcal{E}_h\setminus\Gamma_h} &= 0\,, && \text{(35c)}\\
\langle \boldsymbol{\varepsilon}_{\widehat{\boldsymbol{\sigma}}}\boldsymbol{n}_h, \boldsymbol{\mu}\rangle_{\Gamma_h^N} &= \langle (G - G_h)\boldsymbol{n}\circ\boldsymbol{\phi}, \boldsymbol{\mu}\rangle_{\Gamma_h^N}\,, && \text{(35d)}\\
\langle \boldsymbol{\varepsilon}_{\widehat{\boldsymbol{V}}}, \boldsymbol{\mu}\rangle_{\Gamma_h^D} &= \langle \boldsymbol{g}^D - \boldsymbol{g}_h^D, \boldsymbol{\mu}\rangle_{\Gamma_h^D}\,, && \text{(35e)}\\
\boldsymbol{\varepsilon}_{\widehat{\boldsymbol{\sigma}}}\,\boldsymbol{n}_h &= \boldsymbol{\varepsilon}_{\boldsymbol{\sigma}}\boldsymbol{n}_h + \tau\,(\boldsymbol{\varepsilon}_{\boldsymbol{V}} - \boldsymbol{\varepsilon}_{\widehat{\boldsymbol{V}}})\,, && \text{(35f)}
\end{aligned}
$$

for all $(\boldsymbol{\psi}, \boldsymbol{w}, \boldsymbol{\mu}) \in \mathbb{Z}_h \times \boldsymbol{W}_h \times \boldsymbol{M}_h$.

The following lemma provides a useful representation of the normal component of the error on the deformation field flux $\boldsymbol{\varepsilon}_{\boldsymbol{\sigma}}$.

Lemma 5.2. *Consider the definition in (33). The following equation holds*

$$
\boldsymbol{\varepsilon}_{\boldsymbol{\sigma}}\,\boldsymbol{n}_h = l^{-1}\,(\boldsymbol{g}^D - \boldsymbol{g}_h^D) - \Lambda^{\boldsymbol{I}_{\boldsymbol{\sigma}}} - \Lambda^{\boldsymbol{\varepsilon}_{\boldsymbol{\sigma}}} - \boldsymbol{I}_{\boldsymbol{\sigma}}\,\boldsymbol{n}_h\,. \tag{36}
$$

Proof. Let us note that

$$
\boldsymbol{g}^D - \boldsymbol{g}_h^D = \int_0^{l(\boldsymbol{x})} \boldsymbol{\sigma}(\boldsymbol{x} + s\,\boldsymbol{n}_h)\,ds - \int_0^{l(\boldsymbol{x})} \boldsymbol{E}_h(\boldsymbol{\sigma})(\boldsymbol{x} + s\,\boldsymbol{n}_h)\,ds = \int_0^{l(\boldsymbol{x})} (\boldsymbol{\sigma} - \boldsymbol{E}_h(\boldsymbol{\sigma}))(\boldsymbol{x} + s\,\boldsymbol{n}_h)\,ds\,.
$$

Adding and subtracting $\boldsymbol{\Pi}_{\mathbb{Z}}\boldsymbol{\sigma}$ in the integrand above we get

$$
\begin{aligned}
\boldsymbol{g}^D - \boldsymbol{g}_h^D &= \int_0^{l(\boldsymbol{x})} (I_{\boldsymbol{\sigma}} + \boldsymbol{\varepsilon}_{\boldsymbol{\sigma}})(\boldsymbol{x} + s\,\boldsymbol{n}_h)\,ds\\
&= \int_0^{l(\boldsymbol{x})} (I_{\boldsymbol{\sigma}}(\boldsymbol{x} + s\,\boldsymbol{n}_h) - I_{\boldsymbol{\sigma}}(\boldsymbol{x}))\,\boldsymbol{n}_h\,ds + l(\boldsymbol{x})\,I_{\boldsymbol{\sigma}}(\boldsymbol{x})\,\boldsymbol{n}_h + \int_0^{l(\boldsymbol{x})} (\boldsymbol{\varepsilon}_{\boldsymbol{\sigma}}(\boldsymbol{x} + s\,\boldsymbol{n}_h) - \boldsymbol{\varepsilon}_{\boldsymbol{\sigma}}(\boldsymbol{x}))\,\boldsymbol{n}_h\,ds\\
&\quad + l(\boldsymbol{x})\,\boldsymbol{\varepsilon}_{\boldsymbol{\sigma}}(\boldsymbol{x})\,\boldsymbol{n}_h\\
&= l(\boldsymbol{x})(\Lambda^{I_{\boldsymbol{\sigma}}} + I_{\boldsymbol{\sigma}}\,\boldsymbol{n}_h + \Lambda^{\boldsymbol{\varepsilon}_{\boldsymbol{\sigma}}} + \boldsymbol{\varepsilon}_{\boldsymbol{\sigma}}\,\boldsymbol{n}_h)(\boldsymbol{x})\,,
\end{aligned}
$$

after a rearrangement of terms the result follows. □ □

Now, we present a useful result for the analysis

Lemma 5.3. *Let $\boldsymbol{\varepsilon}_{\boldsymbol{\sigma}}, \boldsymbol{\varepsilon}_{\widehat{\boldsymbol{\sigma}}}, \boldsymbol{\varepsilon}_{\boldsymbol{V}}, \boldsymbol{\varepsilon}_{\widehat{\boldsymbol{V}}}$ be solutions to the system (35); then the following holds:*

$$
\|\boldsymbol{\varepsilon}_{\boldsymbol{\sigma}}\|_{D_h}^2 + \|\tau^{1/2}\,(\boldsymbol{\varepsilon}_{\boldsymbol{V}} - \boldsymbol{\varepsilon}_{\widehat{\boldsymbol{V}}})\|_{\mathcal{E}_h}^2 + \langle \boldsymbol{g}^D - \boldsymbol{g}_h^D, \boldsymbol{\varepsilon}_{\widehat{\boldsymbol{\sigma}}}\,\boldsymbol{n}_h\rangle_{\Gamma_h^D} + \langle (G - G_h)\boldsymbol{n}\circ\boldsymbol{\phi}, \boldsymbol{\varepsilon}_{\widehat{\boldsymbol{V}}}\rangle_{\Gamma_h^N} = -(\boldsymbol{I}_{\boldsymbol{\sigma}}, \boldsymbol{\varepsilon}_{\boldsymbol{\sigma}})_{D_h}\,. \tag{37}
$$

Proof. Setting $\boldsymbol{\psi} = \boldsymbol{\varepsilon}_{\boldsymbol{\sigma}}$ and $\boldsymbol{w} = \boldsymbol{\varepsilon}_{\boldsymbol{V}}$, integrating by parts and adding both equations we obtain

$$
\|\boldsymbol{\varepsilon}_{\boldsymbol{\sigma}}\|_{D_h}^2 + \langle \boldsymbol{\varepsilon}_{\widehat{\boldsymbol{\sigma}}}\,\boldsymbol{n}_h - \boldsymbol{\varepsilon}_{\boldsymbol{\sigma}}\,\boldsymbol{n}_h, \boldsymbol{\varepsilon}_{\boldsymbol{V}}\rangle_{\mathcal{E}_h} + \langle \boldsymbol{\varepsilon}_{\widehat{\boldsymbol{V}}}, \boldsymbol{\varepsilon}_{\boldsymbol{\sigma}}\,\boldsymbol{n}_h\rangle_{\mathcal{E}_h} = -(\boldsymbol{I}_{\boldsymbol{\sigma}}, \boldsymbol{\varepsilon}_{\boldsymbol{\sigma}})_{D_h}\,,
$$

then, by (35f)

$$
\|\boldsymbol{\varepsilon}_{\boldsymbol{\sigma}}\|_{D_h}^2 + \|\tau^{1/2}\,(\boldsymbol{\varepsilon}_{\boldsymbol{V}} - \boldsymbol{\varepsilon}_{\widehat{\boldsymbol{V}}})\|_{\mathcal{E}_h}^2 + \langle \boldsymbol{\varepsilon}_{\widehat{\boldsymbol{\sigma}}}\,\boldsymbol{n}_h, \boldsymbol{\varepsilon}_{\widehat{\boldsymbol{V}}}\rangle_{\mathcal{E}_h} = -(\boldsymbol{I}_{\boldsymbol{\sigma}}, \boldsymbol{\varepsilon}_{\boldsymbol{\sigma}})_{D_h}\,.
$$

Furthermore, note that by (35c), (35d), and (35e) we obtain

$$
\begin{aligned}
\langle \boldsymbol{\varepsilon}_{\widehat{\boldsymbol{\sigma}}}\,\boldsymbol{n}_h, \boldsymbol{\varepsilon}_{\widehat{\boldsymbol{V}}}\rangle_{\mathcal{E}_h} &= \langle \boldsymbol{\varepsilon}_{\widehat{\boldsymbol{\sigma}}}\,\boldsymbol{n}_h, \boldsymbol{\varepsilon}_{\widehat{\boldsymbol{V}}}\rangle_{\mathcal{E}_h\setminus\Gamma_h} + \langle \boldsymbol{\varepsilon}_{\widehat{\boldsymbol{\sigma}}}\,\boldsymbol{n}_h, \boldsymbol{\varepsilon}_{\widehat{\boldsymbol{V}}}\rangle_{\Gamma_h^D} + \langle \boldsymbol{\varepsilon}_{\widehat{\boldsymbol{\sigma}}}\,\boldsymbol{n}_h, \boldsymbol{\varepsilon}_{\widehat{\boldsymbol{V}}}\rangle_{\Gamma_h^N}\\
&= \langle \boldsymbol{g}^D - \boldsymbol{g}_h^D, \boldsymbol{\varepsilon}_{\widehat{\boldsymbol{\sigma}}}\,\boldsymbol{n}_h\rangle_{\Gamma_h^D} + \langle (G - G_h)\boldsymbol{n}\circ\boldsymbol{\phi}, \boldsymbol{\varepsilon}_{\widehat{\boldsymbol{V}}}\rangle_{\Gamma_h^N}\,.
\end{aligned}
$$

and the result follows. □ □

Let us now introduce a key lemma for the error analysis,

Lemma 5.4. *Suppose that $\mathcal{T}_h$ is an admissible triangulation and define*

$$|||(\boldsymbol{\varepsilon_\sigma}, \boldsymbol{\varepsilon_V} - \boldsymbol{\varepsilon_{\widehat{V}}}, \boldsymbol{g}^D - \boldsymbol{g}_h^D)||| := \left(\|\boldsymbol{\varepsilon_\sigma}\|_{D_h}^2 + \|\boldsymbol{\varepsilon_V} - \boldsymbol{\varepsilon_{\widehat{V}}}\|_{\mathcal{E}_h,\tau}^2 + \|\boldsymbol{g}^D - \boldsymbol{g}_h^D\|_{\Gamma_h^D,l^{-1}}^2 \right)^{1/2} . \tag{38}$$

The following inequality holds

$$\begin{aligned} |||(\boldsymbol{\varepsilon_\sigma}, \boldsymbol{\varepsilon_V} - \boldsymbol{\varepsilon_{\widehat{V}}}, \boldsymbol{g}^D - \boldsymbol{g}_h^D)||| \lesssim \|\boldsymbol{I_\sigma}\|_{D_h} + R^{1/2} \|\boldsymbol{I_\sigma} \boldsymbol{n}_h\|_{\Gamma_h^D,h^\perp} + \left\| \left(h^{-1/2} \tfrac{\epsilon}{2} + \tau^{-1/2} \right) (G - G_h) \boldsymbol{n} \circ \boldsymbol{\phi} \right\|_{\Gamma_h^N} \\ + R \|\partial_{\boldsymbol{n}_h} (\boldsymbol{I_\sigma} \boldsymbol{n}_h)\|_{D_h^c,(h^\perp)^2} + \|\tfrac{1}{2\epsilon} C_{tr} \boldsymbol{\varepsilon_V}\|_{D_h} , \end{aligned} \tag{39}$$

with $\epsilon > 0$ a parameter at our disposal and C_{tr} a positive constant independent of h.

Proof. Applying the Cauchy-Schwarz inequality followed by Young's inequality in (37) we get

$$\frac{1}{2} \|\boldsymbol{\varepsilon_\sigma}\|_{D_h}^2 + \|\tau^{1/2} (\boldsymbol{\varepsilon_V} - \boldsymbol{\varepsilon_{\widehat{V}}})\|_{\mathcal{E}_h}^2 + \langle \boldsymbol{g}^D - \boldsymbol{g}_h^D, \boldsymbol{\varepsilon_{\widehat{\sigma}}} \boldsymbol{n}_h \rangle_{\Gamma_h^D} + \langle (G - G_h) \boldsymbol{n} \circ \boldsymbol{\phi}, \boldsymbol{\varepsilon_{\widehat{V}}} \rangle_{\Gamma_h^N} \leq \frac{1}{2} \|\boldsymbol{I_\sigma}\|_{D_h}^2 . \tag{40}$$

On the other hand, note that combining (35f) and (36), the following equation holds,

$$\begin{aligned} \langle \boldsymbol{\varepsilon_{\widehat{\sigma}}} \boldsymbol{n}_h, \boldsymbol{g}^D - \boldsymbol{g}_h^D \rangle_{\Gamma_h^D} &= \|l^{-1/2} (\boldsymbol{g}^D - \boldsymbol{g}_h^D)\|_{\Gamma_h^D}^2 - \langle \Lambda^{\boldsymbol{I_\sigma}}, \boldsymbol{g}^D - \boldsymbol{g}_h^D \rangle_{\Gamma_h^D} - \langle \Lambda^{\boldsymbol{\varepsilon_\sigma}}, \boldsymbol{g}^D - \boldsymbol{g}_h^D \rangle_{\Gamma_h^D} \\ &\quad - \langle \boldsymbol{I_\sigma} \boldsymbol{n}_h, \boldsymbol{g}^D - \boldsymbol{g}_h^D \rangle_{\Gamma_h^D} + \langle \tau (\boldsymbol{\varepsilon_V} - \boldsymbol{\varepsilon_{\widehat{V}}}), \boldsymbol{g}^D - \boldsymbol{g}_h^D \rangle_{\Gamma_h^D} . \end{aligned}$$

Then, substituting the expression obtained above in (40) and performing some algebraic manipulations, we obtain

$$\begin{aligned} &\frac{1}{2} \|\boldsymbol{\varepsilon_\sigma}\|_{D_h}^2 + \|\tau^{1/2} (\boldsymbol{\varepsilon_V} - \boldsymbol{\varepsilon_{\widehat{V}}})\|_{\mathcal{E}_h}^2 + \|l^{-1/2} (\boldsymbol{g}^D - \boldsymbol{g}_h^D)\|_{\Gamma_h^D}^2 \\ &\quad \leq \frac{1}{2} \|\boldsymbol{I_\sigma}\|_{D_h}^2 + \langle \Lambda^{\boldsymbol{I_\sigma}}, \boldsymbol{g}^D - \boldsymbol{g}_h^D \rangle_{\Gamma_h^D} + \langle \Lambda^{\boldsymbol{\varepsilon_\sigma}}, \boldsymbol{g}^D - \boldsymbol{g}_h^D \rangle_{\Gamma_h^D} + \langle \boldsymbol{I_\sigma} \boldsymbol{n}_h, \boldsymbol{g}^D - \boldsymbol{g}_h^D \rangle_{\Gamma_h^D} \\ &\qquad - \langle \tau (\boldsymbol{\varepsilon_V} - \boldsymbol{\varepsilon_{\widehat{V}}}), \boldsymbol{g}^D - \boldsymbol{g}_h^D \rangle_{\Gamma_h^D} - \langle (G - G_h) \boldsymbol{n} \circ \boldsymbol{\phi}, \boldsymbol{\varepsilon_{\widehat{V}}} \rangle_{\Gamma_h^N} \\ &\quad = \frac{1}{2} \|\boldsymbol{I_\sigma}\|_{D_h}^2 \\ &\qquad + \langle \Lambda^{\boldsymbol{I_\sigma}}, \boldsymbol{g}^D - \boldsymbol{g}_h^D \rangle_{\Gamma_h^D} + \langle \Lambda^{\boldsymbol{\varepsilon_\sigma}}, \boldsymbol{g}^D - \boldsymbol{g}_h^D \rangle_{\Gamma_h^D} + \langle \boldsymbol{I_\sigma} \boldsymbol{n}_h, \boldsymbol{g}^D - \boldsymbol{g}_h^D \rangle_{\Gamma_h^D} - \langle \tau (\boldsymbol{\varepsilon_V} - \boldsymbol{\varepsilon_{\widehat{V}}}), \boldsymbol{g}^D - \boldsymbol{g}_h^D \rangle_{\Gamma_h^D} \\ &\qquad + \langle \tau^{1/2} (\boldsymbol{\varepsilon_V} - \boldsymbol{\varepsilon_{\widehat{V}}}), \tau^{-1/2} (G - G_h) \boldsymbol{n} \circ \boldsymbol{\phi} \rangle_{\Gamma_h^N} - \langle \boldsymbol{\varepsilon_V}, (G - G_h) \boldsymbol{n} \circ \boldsymbol{\phi} \rangle_{\Gamma_h^N} . \end{aligned} \tag{41}$$

Focusing on the expression (41), we note that applying successively the Cauchy-Schwarz inequality and Young's $ab \leq \frac{\epsilon}{2} a^2 + \frac{1}{2\epsilon} b^2$ inequality (with constants ϵ_i for $i = 1, 2, 3, 4$) to each of the terms on the the second–to last line above, it follows that

$$\begin{aligned} &\langle \Lambda^{\boldsymbol{I_\sigma}}, \boldsymbol{g}^D - \boldsymbol{g}_h^D \rangle_{\Gamma_h^D} + \langle \Lambda^{\boldsymbol{\varepsilon_\sigma}}, \boldsymbol{g}^D - \boldsymbol{g}_h^D \rangle_{\Gamma_h^D} + \langle \boldsymbol{I_\sigma} \boldsymbol{n}_h, \boldsymbol{g}^D - \boldsymbol{g}_h^D \rangle_{\Gamma_h^D} - \langle \tau (\boldsymbol{\varepsilon_V} - \boldsymbol{\varepsilon_{\widehat{V}}}), \boldsymbol{g}^D - \boldsymbol{g}_h^D \rangle_{\Gamma_h^D} \\ &\quad \leq \frac{1}{2\epsilon_1} \|l^{1/2} \Lambda^{\boldsymbol{I_\sigma}}\|_{\Gamma_h^D}^2 + \frac{1}{2\epsilon_2} \|l^{1/2} \Lambda^{\boldsymbol{\varepsilon_\sigma}}\|_{\Gamma_h^D}^2 + \frac{1}{2\epsilon_3} \|l^{1/2} \boldsymbol{I_\sigma} \boldsymbol{n}_h\|_{\Gamma_h^D}^2 + \frac{1}{2\epsilon_4} \|l^{1/2} \tau (\boldsymbol{\varepsilon_V} - \boldsymbol{\varepsilon_{\widehat{V}}})\|_{\Gamma_h^D}^2 \\ &\qquad + \frac{1}{2} (\epsilon_1 + \epsilon_2 + \epsilon_3 + \epsilon_4) \|l^{-1/2} (\boldsymbol{g}^D - \boldsymbol{g}_h^D)\|_{\Gamma_h^D}^2 \\ &\quad = 3 (\|l^{1/2} \Lambda^{\boldsymbol{I_\sigma}}\|_{\Gamma_h^D}^2 + \|l^{1/2} \Lambda^{\boldsymbol{\varepsilon_\sigma}}\|_{\Gamma_h^D}^2 + \|l^{1/2} \boldsymbol{I_\sigma} \boldsymbol{n}_h\|_{\Gamma_h^D}^2) + \frac{1}{2} \|l^{1/2} \tau (\boldsymbol{\varepsilon_V} - \boldsymbol{\varepsilon_{\widehat{V}}})\|_{\Gamma_h^D}^2 + \frac{3}{4} \|l^{-1/2} (\boldsymbol{g}^D - \boldsymbol{g}_h^D)\|_{\Gamma_h^D}^2 , \end{aligned} \tag{42}$$

where we have chosen $\epsilon_1 = \epsilon_2 = \epsilon_3 = 1/6$ and $\epsilon_4 = 1$. By a similar argument we have for the last line in (41),

$$\begin{aligned} &\langle \tau^{1/2} (\boldsymbol{\varepsilon_V} - \boldsymbol{\varepsilon_{\widehat{V}}}), \tau^{-1/2} (G - G_h) \boldsymbol{n} \circ \boldsymbol{\phi} \rangle_{\Gamma_h^N} - \langle \boldsymbol{\varepsilon_V}, (G - G_h) \boldsymbol{n} \circ \boldsymbol{\phi} \rangle_{\Gamma_h^N} \\ &\quad \leq \left\| \left(h^{-1/2} \tfrac{\epsilon}{2} + \tau^{-1/2} \right) (G - G_h) \boldsymbol{n} \circ \boldsymbol{\phi} \right\|_{\Gamma_h^N}^2 + \tfrac{1}{4} \|\tau^{1/2} (\boldsymbol{\varepsilon_V} - \boldsymbol{\varepsilon_{\widehat{V}}})\|_{\Gamma_h^N}^2 + \left\| \tfrac{1}{2\epsilon} h^{1/2} \boldsymbol{\varepsilon_V} \right\|_{\Gamma_h^N}^2 \quad \text{(Cauchy-Schwarz \& Young)} \\ &\quad \leq \left\| \left(h^{-1/2} \tfrac{\epsilon}{2} + \tau^{-1/2} \right) (G - G_h) \boldsymbol{n} \circ \boldsymbol{\phi} \right\|_{\Gamma_h^N}^2 + \tfrac{1}{4} \|\tau^{1/2} (\boldsymbol{\varepsilon_V} - \boldsymbol{\varepsilon_{\widehat{V}}})\|_{\Gamma_h^N}^2 + \left\| \tfrac{1}{2\epsilon} C_{tr} \boldsymbol{\varepsilon_V} \right\|_{D_h}^2 \quad \text{(discrete trace inequality)} , \end{aligned} \tag{43}$$

with $\epsilon > 0$ a parameter at our disposal. Substituting the estimates (42) and (43) into (41) it follows that

$$\begin{aligned}
&\frac{1}{2}\,\|\boldsymbol{\varepsilon_\sigma}\|^2_{D_h} + \frac{1}{4}\,\|\tau^{1/2}\,(\boldsymbol{\varepsilon_V} - \boldsymbol{\varepsilon_{\widehat{V}}})\|^2_{\mathcal{E}_h} \;+\; \frac{1}{4}\,\|l^{-1/2}\,(\boldsymbol{g}^D - \boldsymbol{g}^D_h)\|_{\Gamma^D_h} \\
&\qquad \leq \frac{1}{2}\,\|\boldsymbol{I_\sigma}\|^2_{D_h} \;+\; 3\,\|l^{1/2}\,\Lambda^{\boldsymbol{I_\sigma}}\|^2_{\Gamma^D_h} \;+\; 3\,\|l^{1/2}\,\Lambda^{\boldsymbol{\varepsilon_\sigma}}\|^2_{\Gamma^D_h} \;+\; 3\,\|l^{1/2}\,\boldsymbol{I_\sigma}\boldsymbol{n}_h\|^2_{\Gamma^D_h} \\
&\qquad\quad + \left\|\left(h^{-1/2}\tfrac{\epsilon}{2} + \tau^{-1/2}\right)(G - G_h)\boldsymbol{n}\circ\boldsymbol{\phi}\right\|^2_{\Gamma^N_h} + \left\|\tfrac{1}{2\epsilon}C_{tr}\boldsymbol{\varepsilon_V}\right\|^2_{D_h}\,.
\end{aligned}$$

Then applying (55), (56), and taking into account that $l(\boldsymbol{x}) \leq H_e^\perp = r_e\,h_e^\perp$, we find

$$\begin{aligned}
&\frac{1}{2}\,\|\boldsymbol{\varepsilon_\sigma}\|^2_{D_h} + \frac{1}{4}\,\|\tau^{1/2}\,(\boldsymbol{\varepsilon_V} - \boldsymbol{\varepsilon_{\widehat{V}}})\|^2_{\mathcal{E}_h} \;+\; \frac{1}{4}\,\|l^{-1/2}\,(\boldsymbol{g}^D - \boldsymbol{g}^D_h)\|_{\Gamma^D_h} \\
&\qquad \leq \frac{1}{2}\,\|\boldsymbol{I_\sigma}\|^2_{D_h} \;+\; R^2\,\|\partial_{\boldsymbol{n_h}}(\boldsymbol{I_\sigma}\boldsymbol{n}_h)\|^2_{D^c_h,(h^\perp)^2} \;+\; R^3(C_e^{ext}C_e^{inv})^2\|\boldsymbol{\varepsilon_\sigma}\|^2_{D_h} \;+\; 3\,\|r_e^{1/2}(h_e^\perp)^{1/2}\boldsymbol{I_\sigma}\boldsymbol{n}_h\|^2_{\Gamma^D_h} \\
&\qquad\quad + \left\|\left(h^{-1/2}\tfrac{\epsilon}{2} + \tau^{-1/2}\right)(G - G_h)\boldsymbol{n}\circ\boldsymbol{\phi}\right\|^2_{\Gamma^N_h} + \left\|\tfrac{1}{2\epsilon}C_{tr}\boldsymbol{\varepsilon_V}\right\|^2_{D_h} \\
&\qquad \leq \frac{1}{2}\,\|\boldsymbol{I_\sigma}\|^2_{D_h} \;+\; R^2\,\|\partial_{\boldsymbol{n_h}}(\boldsymbol{I_\sigma}\boldsymbol{n}_h)\|^2_{D^c_h,(h^\perp)^2} \;+\; R^3(C_e^{ext}C_e^{inv})^2\|\boldsymbol{\varepsilon_\sigma}\|^2_{D_h} \;+\; 3\,R\,\|\boldsymbol{I_\sigma}\boldsymbol{n}_h\|^2_{\Gamma^D_h,h^\perp} \\
&\qquad\quad + \left\|\left(h^{-1/2}\tfrac{\epsilon}{2} + \tau^{-1/2}\right)(G - G_h)\boldsymbol{n}\circ\boldsymbol{\phi}\right\|^2_{\Gamma^N_h} + \left\|\tfrac{1}{2\epsilon}C_{tr}\boldsymbol{\varepsilon_V}\right\|^2_{D_h}\,.
\end{aligned}$$

Finally, by (17), we have that $R^3(C_e^{ext}C_e^{inv})^2 < 1/2$, and rearranging terms, (39) holds. □ □

To derive the estimates for $\|\boldsymbol{\varepsilon_\sigma}\|_{D_h}$ we need to control the term $\|(G-G_h)\boldsymbol{n}\circ\boldsymbol{\phi}\|_{\Gamma^N_h}$. We achieve that in the following lemma.

Lemma 5.5. *Let $\boldsymbol{p}$ and $\boldsymbol{r}$ be the solutions of the state problem (20) and adjoint problem (21), respectively. There exists a positive constant C_G such that*

$$\begin{aligned}
\|(G(\Gamma) - G_h(\Gamma))\boldsymbol{n}\circ\boldsymbol{\phi}\|_{\Gamma^N_h} \leq C_G\big(&\|(\boldsymbol{r}-\boldsymbol{r}_h)\cdot\boldsymbol{n}\|_{\Gamma_N}\|(\boldsymbol{p}-\boldsymbol{p}_h)\cdot\boldsymbol{n}\|_{\Gamma_N} \\
&+\|\boldsymbol{r}\|_{\boldsymbol{H}^1(\Omega)}\,\|(\boldsymbol{p}-\boldsymbol{p}_h)\cdot\boldsymbol{n}\|_{\Gamma_N} + \|\boldsymbol{p}\|_{\boldsymbol{H}^1(\Omega)}\,\|(\boldsymbol{r}-\boldsymbol{r}_h)\cdot\boldsymbol{n}\|_{\Gamma_N} + \|(\boldsymbol{r}-\boldsymbol{r}_h)\cdot\boldsymbol{n}\|_{\Gamma_N}\big)\,,
\end{aligned} \tag{44}$$

Furthermore, for $\boldsymbol{q} \in \{\boldsymbol{p}, \boldsymbol{r}\}$, there holds

$$\|(\boldsymbol{q}-\boldsymbol{q}_h)\cdot\boldsymbol{n}\|_{\Gamma_N} \lesssim h^{m+1/2}(\|\boldsymbol{q}\|_{\boldsymbol{H}^{m+1}(\Omega)} + |y|_{H^{k+1}(\Omega)}) + h^{-1/2}\|\boldsymbol{I_q}\|_{D_h} + Rh^{-1/2}\|\boldsymbol{\varepsilon_q}\|_{D_h}\,. \tag{45}$$

Proof. Let us note the following

$$G(\Gamma) \;-\; G_h(\Gamma) \;=\; a^{-1}\,(\boldsymbol{p}\cdot\boldsymbol{n}\,\boldsymbol{r}\cdot\boldsymbol{n} - \boldsymbol{p}_h\cdot\boldsymbol{n}\,\boldsymbol{r}_h\cdot\boldsymbol{n}) \;+\; \partial_{\boldsymbol{n}}g\,(\boldsymbol{r}-\boldsymbol{r}_h)\cdot\boldsymbol{n}\,,$$

hence, we have that

$$\begin{aligned}
\|(G-G_h)\boldsymbol{n}\circ\boldsymbol{\phi}\|_{\Gamma^N_h} &\lesssim \|(G-G_h)\boldsymbol{n}\|_{\Gamma_N} \lesssim \|G_h - G\|_{\Gamma_N} \\
&\lesssim \|\boldsymbol{p}\cdot\boldsymbol{n}\,\boldsymbol{r}\cdot\boldsymbol{n} - \boldsymbol{p}_h\cdot\boldsymbol{n}\,\boldsymbol{r}_h\cdot\boldsymbol{n}\|_{\Gamma_N} \;+\; \|(\boldsymbol{r}-\boldsymbol{r}_h)\cdot\boldsymbol{n}\|_{\Gamma_N} \\
&\lesssim \|\boldsymbol{p}\cdot\boldsymbol{n}\,(\boldsymbol{r}-\boldsymbol{r}_h)\cdot\boldsymbol{n}\|_{\Gamma_N} \;+\; \|\boldsymbol{r}_h\cdot\boldsymbol{n}\,(\boldsymbol{p}-\boldsymbol{p}_h)\cdot\boldsymbol{n}\|_{\Gamma_N} \;+\; \|(\boldsymbol{r}-\boldsymbol{r}_h)\cdot\boldsymbol{n}\|_{\Gamma_N} \\
&\lesssim \|\boldsymbol{p}\cdot\boldsymbol{n}\|_{\Gamma_N}\,\|(\boldsymbol{r}-\boldsymbol{r}_h)\cdot\boldsymbol{n}\|_{\Gamma_N} \;+\|(\boldsymbol{r}-\boldsymbol{r}_h)\cdot\boldsymbol{n}\|_{\Gamma_N}\,\|(\boldsymbol{p}\;-\boldsymbol{p}_h)\cdot\boldsymbol{n}\|_{\Gamma_N} \\
&\quad + \|\boldsymbol{r}\cdot\boldsymbol{n}\|_{\Gamma_N}\,\|(\boldsymbol{p}-\boldsymbol{p}_h)\cdot\boldsymbol{n}\|_{\Gamma_N} \;+\; \|(\boldsymbol{r}-\boldsymbol{r}_h)\cdot\boldsymbol{n}\|_{\Gamma_N}\,.
\end{aligned}$$

Then, (44) follows by the continuous trace inequality. On the other hand, we will prove the bound of the statement only for $\|(\boldsymbol{p}-\boldsymbol{p}_h)\cdot\boldsymbol{n}\|_{\Gamma_N}$, since the proof for the bound of $\|(\boldsymbol{r}-\boldsymbol{r}_h)\cdot\boldsymbol{n}\|_{\Gamma_N}$ is analogous.

Let $\Gamma_e \subset \Gamma_N$. By adding and subtracting $\boldsymbol{E}(\Pi_{\boldsymbol{Z}}\boldsymbol{p})$ we have that

$$h_e^{1/2}\|(\boldsymbol{p}-\boldsymbol{p}_h)\cdot\boldsymbol{n}\|_{\Gamma_e} \leq h_e^{1/2}\|\boldsymbol{p} - \boldsymbol{E}(\Pi_{\boldsymbol{Z}}\boldsymbol{p})\|_{\Gamma_e} + h_e^{1/2}\|\boldsymbol{E}(\Pi_{\boldsymbol{Z}}\boldsymbol{p}) - \boldsymbol{p}_h\|_{\Gamma_e}\,.$$

We bound the first term of the right hand side of the above equation by (59), and by (58), we bound the second term of the above equation, thus obtaining

$$h_e^{1/2}\,\|(\boldsymbol{p}-\boldsymbol{p}_h)\cdot\boldsymbol{n}\|_{\Gamma_e} \lesssim \|\boldsymbol{I_p}\|_{K_e^{ext}\cup K_e} + h_e\|\nabla\boldsymbol{I_p}\|_{K_e^{ext}\cup K_e} + \|\boldsymbol{\varepsilon_p}\|_{K_e^{ext}}\,,$$

In turn we note that using the definition of C_e^{ext} (see [24, Lemma A.1]), we have that $\|\boldsymbol{\varepsilon_p}\|_{K_e^{ext}} \lesssim r_e^{1/2}\|\boldsymbol{\varepsilon_p}\|_{K_e}$, thus we deduce

$$\begin{aligned}
h_e^{1/2}\|(\boldsymbol{p}-\boldsymbol{p}_h)\cdot\boldsymbol{n}\|_{\Gamma_e} &\lesssim \|\boldsymbol{I_p}\|_{K_e^{ext}\cup K_e} + h_e\|\nabla \boldsymbol{I_p}\|_{K_e^{ext}\cup K_e} + r_e^{1/2}\|\boldsymbol{\varepsilon_p}\|_{K_e} \\
&\lesssim \|\boldsymbol{I_p}\|_{K_e^{ext}\cup K_e} + h_e^{m+1}|\boldsymbol{E}(\boldsymbol{p})|_{\boldsymbol{H}^{m+1}(B_e)} + r_e^{1/2}h_e^{m+1}\|\boldsymbol{E}(\boldsymbol{p})\|_{\boldsymbol{H}^{m+1}(K_e)} \\
&\quad + r_e^{1/2}\|\boldsymbol{I_p}\|_{K_e} + h_e\|\nabla \boldsymbol{I_p}\|_{K_e} + r_e^{1/2}\,\|\boldsymbol{\varepsilon_p}\|_{K_e}. && \text{(by (62))} \\
&\lesssim (1+r_e^{1/2})h^{m+1}\|\boldsymbol{E}(\boldsymbol{p})\|_{\boldsymbol{H}^{m+1}(B_e)} + (1+r_e^{1/2})\|\boldsymbol{I_p}\|_{K_e} + h_e\|\nabla \boldsymbol{I_p}\|_{K_e} + r_e^{1/2}\|\boldsymbol{\varepsilon_p}\|_{K_e}\,. && \text{(by (61))}
\end{aligned}$$

Dividing by $h_e^{1/2}$, adding over all the elements and applying (60), (67), and bearing in mind the definition of R and h, (45) holds. □

We can note that the fourth term on the right hand side in (39) is controlled by [24, Lemma 3.8]. Then, the unique term that is not controlled is $\|\boldsymbol{\varepsilon_V}\|_{D_h}$. In order to have an estimate for the latter we have to present the error estimates for $\boldsymbol{V}-\boldsymbol{V}_h$, which is presented in the next section. Once we have performed this analysis, we will be in position to establish the error estimates for the deformation field equation.

5.3 Error estimates for $\boldsymbol{V}-\boldsymbol{V}_h$

In this section we develop the error estimates for $\boldsymbol{V}-\boldsymbol{V}_h$, for this purpose we will follow the same strategy done for the estimates of e^y and e^z, i.e., we will use a dual problem to find the estimates. For any given $\boldsymbol{U}\in[L^2(\Omega)]^d$, let be $(\boldsymbol{\gamma},\boldsymbol{u})$ solution of

$$\begin{aligned}
\boldsymbol{\gamma} + \nabla\boldsymbol{u} &= 0 \quad \text{in } D_h\,, && \text{(46a)}\\
\mathbf{div}(\boldsymbol{\gamma}) &= \boldsymbol{U} \quad \text{in } D_h\,, && \text{(46b)}\\
\boldsymbol{u} &= \boldsymbol{0} \quad \text{on } \Gamma_h^D\,, && \text{(46c)}\\
\boldsymbol{\gamma}\,\boldsymbol{n}_h &= \boldsymbol{0} \quad \text{on } \Gamma_h^N\,. && \text{(46d)}
\end{aligned}$$

We assume that the solution to this dual problem satisfies the elliptic regularity

$$\|\boldsymbol{u}\|_{s+1,D_h} + \|\boldsymbol{\gamma}\|_{s,D_h} \le C\,\|\boldsymbol{U}\|_{D_h}\,, \tag{47}$$

where $s\ge 0$, and $C>0$ depend on the domain D_h.

Remark 1. *The elliptic regularity holds with $s=1$, for example, when the domain is a convex polyhedral or has a $\mathcal{C}^2$ boundary as in [24]. This H^2-regularity is usually used to prove superconvergence properties of HDG schemes. However, since in our context the domain D_h might be a nonconvex polyhedron, the purpose of this duality argument is not to show suerconvergence but rather to to bound $\|\boldsymbol{\varepsilon_V}\|_{D_h}$ and obtain error estimates even for the case $s=0$.*

We have the following identity.

Lemma 5.6. *The projection of the errors and the interpolation errors satisfy the following identity*

$$(\boldsymbol{\varepsilon_V},\boldsymbol{U})_{D_h} = (\boldsymbol{I_\sigma},\boldsymbol{\Pi}_{\mathbb{Z}}\boldsymbol{\gamma})_{D_h} - (\boldsymbol{\varepsilon_\sigma},\boldsymbol{\gamma}-\boldsymbol{\Pi}_{\mathbb{Z}}\boldsymbol{\gamma})_{D_h} + \mathbb{T}_{\boldsymbol{V},h}\,, \tag{48}$$

where

$$\mathbb{T}_{\boldsymbol{V},h} := \langle \boldsymbol{g}^D - \boldsymbol{g}_h^D, \boldsymbol{\gamma}\,\boldsymbol{n}_h\rangle_{\Gamma_h^D} - \langle (G-G_h)\boldsymbol{n}\circ\boldsymbol{\phi},\boldsymbol{u}\rangle_{\Gamma_h^N}\,. \tag{49}$$

Proof. Let us note that bearing in mind (46a), (46b), we get

$$\begin{aligned}
(\boldsymbol{\varepsilon_V},\boldsymbol{U})_{D_h} &= (\boldsymbol{\varepsilon_V},\mathbf{div}(\boldsymbol{\gamma}))_{D_h} = (\boldsymbol{\varepsilon_V},\mathbf{div}(\boldsymbol{\gamma}))_{D_h} - (\boldsymbol{\varepsilon_\sigma},\boldsymbol{\gamma})_{D_h} - (\boldsymbol{\varepsilon_\sigma},\nabla\boldsymbol{u})_{D_h}\\
&= (\boldsymbol{\varepsilon_V},\mathbf{div}(\boldsymbol{\Pi}_{\mathbb{Z}}\boldsymbol{\gamma}))_{D_h} + (\boldsymbol{\varepsilon_V},\mathbf{div}(\boldsymbol{\gamma}-\boldsymbol{\Pi}_{\mathbb{Z}}\boldsymbol{\gamma}))_{D_h} - (\boldsymbol{\varepsilon_\sigma},\boldsymbol{\Pi}_{\mathbb{Z}}\boldsymbol{\gamma})_{D_h} - (\boldsymbol{\varepsilon_\sigma},\boldsymbol{\gamma}-\boldsymbol{\Pi}_{\mathbb{Z}}\boldsymbol{\gamma})_{D_h}\\
&\quad - (\boldsymbol{\varepsilon_\sigma},\nabla\boldsymbol{\Pi}_{\boldsymbol{W}}\boldsymbol{u})_{D_h} - (\boldsymbol{\varepsilon_\sigma},\nabla(\boldsymbol{u}-\boldsymbol{\Pi}_{\boldsymbol{W}}\boldsymbol{u}))_{D_h}\,.
\end{aligned}$$

Setting $\boldsymbol{\psi}=\boldsymbol{\Pi}_{\mathbb{Z}}\boldsymbol{\gamma}$ in (35a) and $\boldsymbol{w}=\boldsymbol{\Pi}_{\boldsymbol{W}}\boldsymbol{u}$ in (35b), implies that

$$(\boldsymbol{\varepsilon_V},\boldsymbol{U})_{D_h} = (\boldsymbol{I_\sigma},\boldsymbol{\Pi}_{\mathbb{Z}}\boldsymbol{\gamma})_{D_h} - (\boldsymbol{\varepsilon_\sigma},\boldsymbol{\gamma}-\Pi_{\mathbb{Z}}\boldsymbol{\gamma})_{D_h} + \mathbb{T}_{\boldsymbol{V},h}\,,$$

where $\mathbb{T}_{\boldsymbol{V},h}$ is defined as

$$\mathbb{T}_{\boldsymbol{V},h} := \langle \boldsymbol{\varepsilon}_{\boldsymbol{V}}, \boldsymbol{\Pi}_{\mathbb{Z}}\boldsymbol{\gamma}\,\boldsymbol{n}_h\rangle_{\mathcal{E}_h} - \langle \boldsymbol{\varepsilon}_{\widehat{\boldsymbol{\sigma}}}\,\boldsymbol{n}_h, \boldsymbol{\Pi}_{\boldsymbol{W}}\boldsymbol{u}\rangle_{\mathcal{E}_h} + (\boldsymbol{\varepsilon}_{\boldsymbol{V}}, \mathbf{div}(\boldsymbol{\gamma} - \boldsymbol{\Pi}_{\mathbb{Z}}\boldsymbol{\gamma}))_{D_h} - (\boldsymbol{\varepsilon}_{\boldsymbol{\sigma}}, \nabla(\boldsymbol{u} - \boldsymbol{\Pi}_{\boldsymbol{W}}\boldsymbol{u}))_{D_h}.$$

Integrating by parts we can deduce

$$\begin{aligned}
\mathbb{T}_{\boldsymbol{V},h} &= \langle \boldsymbol{\varepsilon}_{\boldsymbol{V}}, \boldsymbol{\Pi}_{\mathbb{Z}}\boldsymbol{\gamma}\boldsymbol{n}_h\rangle_{\mathcal{E}_h} - \langle \boldsymbol{\varepsilon}_{\widehat{\boldsymbol{\sigma}}}\boldsymbol{n}_h, \boldsymbol{\Pi}_{\boldsymbol{W}}\boldsymbol{u}\rangle_{\mathcal{E}_h} - (\nabla\boldsymbol{\varepsilon}_{\boldsymbol{V}}, \boldsymbol{\gamma} - \boldsymbol{\Pi}_{\mathbb{Z}}\boldsymbol{\gamma})_{D_h} + \langle \boldsymbol{\varepsilon}_{\boldsymbol{V}}, \boldsymbol{\gamma} - \boldsymbol{\Pi}_{\mathbb{Z}}\boldsymbol{\gamma}\rangle_{\mathcal{E}_h} \\
&\quad + (\mathbf{div}(\boldsymbol{\varepsilon}_{\boldsymbol{\sigma}}), \boldsymbol{u} - \boldsymbol{\Pi}_{\boldsymbol{W}}\boldsymbol{u})_{D_h} - \langle \boldsymbol{\varepsilon}_{\boldsymbol{\sigma}}\boldsymbol{n}_h, \boldsymbol{u} - \boldsymbol{\Pi}_{\boldsymbol{W}}\boldsymbol{u}\rangle_{\mathcal{E}_h} \\
&= \langle \boldsymbol{\varepsilon}_{\boldsymbol{V}}, \boldsymbol{\Pi}_{\mathbb{Z}}\boldsymbol{\gamma}\boldsymbol{n}_h\rangle_{\mathcal{E}_h} - \langle \boldsymbol{\varepsilon}_{\widehat{\boldsymbol{\sigma}}}\boldsymbol{n}_h, \boldsymbol{\Pi}_{\boldsymbol{W}}\boldsymbol{u}\rangle_{\mathcal{E}_h} + \langle \boldsymbol{\varepsilon}_{\boldsymbol{V}}, \boldsymbol{\gamma} - \boldsymbol{\Pi}_{\mathbb{Z}}\boldsymbol{\gamma}\rangle_{\mathcal{E}_h} \\
&\quad - \langle \boldsymbol{\varepsilon}_{\boldsymbol{\sigma}}\boldsymbol{n}_h, \boldsymbol{u} - \boldsymbol{\Pi}_{\boldsymbol{W}}\boldsymbol{u}\rangle_{\mathcal{E}_h} \qquad \text{(by (63a) and (63b))} \\
&= \langle \boldsymbol{\varepsilon}_{\widehat{\boldsymbol{V}}} - \boldsymbol{\varepsilon}_{\boldsymbol{V}}, (\boldsymbol{\Pi}_{\mathbb{Z}}\boldsymbol{\gamma} - \boldsymbol{\gamma})\,\boldsymbol{n}_h\rangle_{\mathcal{E}_h} - \langle (\boldsymbol{\varepsilon}_{\widehat{\boldsymbol{\sigma}}} - \boldsymbol{\varepsilon}_{\boldsymbol{\sigma}})\,\boldsymbol{n}_h, \boldsymbol{\Pi}_{\boldsymbol{W}}\boldsymbol{u} - \boldsymbol{u}\rangle_{\mathcal{E}_h} + \langle \boldsymbol{\varepsilon}_{\widehat{\boldsymbol{V}}}, \boldsymbol{\gamma}\,\boldsymbol{n}_h\rangle_{\mathcal{E}_h} - \langle \boldsymbol{\varepsilon}_{\widehat{\boldsymbol{\sigma}}}\,\boldsymbol{n}_h, \boldsymbol{u}\rangle_{\mathcal{E}_h}.
\end{aligned}$$

By (35c) we have that $\langle \boldsymbol{\varepsilon}_{\widehat{\boldsymbol{\sigma}}}\,\boldsymbol{n}_h, \boldsymbol{u}\rangle_{\mathcal{E}_h\setminus\Gamma_h} = 0$. Moreover, since $\boldsymbol{\varepsilon}_{\widehat{\boldsymbol{V}}}$ is single-valued in $\mathcal{E}_h$ and $\boldsymbol{\gamma} \in H(\mathbf{div};\Omega)$, it follows that $\langle \boldsymbol{\varepsilon}_{\widehat{\boldsymbol{V}}}, \boldsymbol{\gamma}\,\boldsymbol{n}_h\rangle_{\mathcal{E}_h} = \langle \boldsymbol{\varepsilon}_{\widehat{\boldsymbol{V}}}, \boldsymbol{\gamma}\,\boldsymbol{n}_h\rangle_{\Gamma_h}$. In turn, by (35f) we obtain

$$\mathbb{T}_{\boldsymbol{V},h} = \langle \boldsymbol{\varepsilon}_{\widehat{\boldsymbol{V}}} - \boldsymbol{\varepsilon}_{\boldsymbol{V}}, (\boldsymbol{\Pi}_{\mathbb{Z}}\boldsymbol{\gamma} - \boldsymbol{\gamma})\,\boldsymbol{n}_h + \tau\,(\boldsymbol{\Pi}_{\boldsymbol{W}}\boldsymbol{u} - \boldsymbol{u})\rangle_{\mathcal{E}_h} + \langle \boldsymbol{\varepsilon}_{\widehat{\boldsymbol{V}}}, \boldsymbol{\gamma}\,\boldsymbol{n}_h\rangle_{\Gamma_h} - \langle \boldsymbol{\varepsilon}_{\widehat{\boldsymbol{\sigma}}}\,\boldsymbol{n}_h, \boldsymbol{u}\rangle_{\Gamma_h}.$$

We note by (63c) that $\langle \boldsymbol{\varepsilon}_{\widehat{\boldsymbol{V}}} - \boldsymbol{\varepsilon}_{\boldsymbol{V}}, (\boldsymbol{\Pi}_{\mathbb{Z}}\boldsymbol{\gamma} - \boldsymbol{\gamma})\,\boldsymbol{n}_h + \tau\,(\boldsymbol{\Pi}_{\boldsymbol{W}}\boldsymbol{u} - \boldsymbol{u})\rangle_{\mathcal{E}_h} = 0$. Finally by (35d), (35e), (46c), and (46d) we get

$$\mathbb{T}_{\boldsymbol{V},h} = \langle \boldsymbol{g}^D - \boldsymbol{g}_h^D, \boldsymbol{\gamma}\,\boldsymbol{n}_h\rangle_{\Gamma_h^D} - \langle (G - G_h)\boldsymbol{n}\circ\boldsymbol{\phi}, \boldsymbol{u}\rangle_{\Gamma_h^N}.$$

□ □

We can now establish one of the most important results of this section. In fact, thanks to this lemma, we will be able to deduce the convergence rate of the scheme.

Lemma 5.7. *Suppose that $\mathcal{T}_h$ is an admissible triangulation and assume the local proximity condition (13) is satisfied for $n \geq 1$ and $0 < \delta < 1$ and $s \geq 0$ in (47). Then,*

$$\begin{aligned}
\|\boldsymbol{\varepsilon}_{\boldsymbol{V}}\|_{D_h} \lesssim \big(&H_{\boldsymbol{V}}\|\boldsymbol{I}_{\boldsymbol{\sigma}}\|_{D_h} + h^{n+\delta}H_{\boldsymbol{V}}\|\partial_{\boldsymbol{n}_h}(\boldsymbol{I}_{\boldsymbol{\sigma}}\boldsymbol{n}_h)\|_{D_h^c,(h^\perp)^2} + h^{n/2+\delta/2}H_{\boldsymbol{V}}\|\boldsymbol{I}_{\boldsymbol{\sigma}}\boldsymbol{n}_h\|_{\Gamma_h^D,h^\perp} \\
&+ (H_{\boldsymbol{V}}^2 h^{-1/2} + 1)\|(G - G_h)\boldsymbol{n}\circ\boldsymbol{\phi}\|_{\Gamma_h^N}\big),
\end{aligned} \tag{50}$$

where $H_{\boldsymbol{V}} := h^s + h^{n/2+\delta/2-1/2}$.

Proof. From Lemma 5.6, we find

$$\begin{aligned}
\mathbb{T}_{\boldsymbol{V},h} =& \langle \boldsymbol{g}^D - \boldsymbol{g}_h^D, \boldsymbol{\gamma}\boldsymbol{n}_h\rangle_{\Gamma_h^D} - \langle (G - G_h)\boldsymbol{n}\circ\boldsymbol{\phi}, \boldsymbol{u}\rangle_{\Gamma_h^N} \\
\leq& \|l^{-1/2}(\boldsymbol{g}^D - \boldsymbol{g}_h^D)\|_{\Gamma_h^D}\|l^{1/2}\boldsymbol{\gamma}\boldsymbol{n}_h\|_{\Gamma_h^D} + \|(G - G_h)\boldsymbol{n}\circ\boldsymbol{\phi}\|_{\Gamma_h^N}\|\boldsymbol{u}\|_{\Gamma_h^N}.
\end{aligned}$$

Adding and subtracting $\boldsymbol{\Pi}_{\mathbb{Z}}\boldsymbol{\gamma}$, using (65) and recalling that $l(\boldsymbol{x}) := |\boldsymbol{x} - \bar{\boldsymbol{x}}| \lesssim h^{n+\delta}$, we obtain

$$\begin{aligned}
\mathbb{T}_{\boldsymbol{V},h} \leq& \|l^{-1/2}(\boldsymbol{g}^D - \boldsymbol{g}_h^D)\|_{\Gamma_h^D}\|l^{1/2}(\boldsymbol{\Pi}_{\mathbb{Z}}\boldsymbol{\gamma} - \boldsymbol{\gamma})\|_{\Gamma_h^D} + \|l^{-1/2}(\boldsymbol{g}^D - \boldsymbol{g}_h^D)\|_{\Gamma_h^D}\|l^{1/2}\boldsymbol{\Pi}_{\mathbb{Z}}\boldsymbol{\gamma}\|_{\Gamma_h^D} \\
&+ \|(G - G_h)\boldsymbol{n}\circ\boldsymbol{\phi}\|_{\Gamma_h^N}\|\boldsymbol{u}\|_{\Gamma_h^N} \\
\lesssim& h^{n/2+\delta/2+s-1/2}\|l^{-1/2}(\boldsymbol{g}^D - \boldsymbol{g}_h^D)\|_{\Gamma_h^D}\|\boldsymbol{U}\|_{D_h} + h^{n/2+\delta/2-1/2}\|l^{-1/2}(\boldsymbol{g}^D - \boldsymbol{g}_h^D)\|_{\Gamma_h^D}\|\boldsymbol{U}\|_{D_h} \\
&+ \|(G - G_h)\boldsymbol{n}\circ\boldsymbol{\phi}\|_{\Gamma_h^N}\|\boldsymbol{U}\|_{D_h} \\
\lesssim& h^{n/2+\delta/2-1/2}\|l^{-1/2}(\boldsymbol{g}^D - \boldsymbol{g}_h^D)\|_{\Gamma_h^D}\|\boldsymbol{U}\|_{D_h} + \|(G - G_h)\boldsymbol{n}\circ\boldsymbol{\phi}\|_{\Gamma_h^N}\|\boldsymbol{U}\|_{D_h}.
\end{aligned} \tag{51}$$

On the other hand, mimicking [24, Step 4 of the proof of Lemma 3.5], we deduce

$$(\boldsymbol{I}_{\boldsymbol{\sigma}}, \boldsymbol{\Pi}_{\mathbb{Z}}\boldsymbol{\gamma})_{D_h} + (\boldsymbol{\varepsilon}_{\boldsymbol{\sigma}}, \boldsymbol{\Pi}_{\mathbb{Z}}\boldsymbol{\gamma} - \boldsymbol{\gamma})_{D_h} \lesssim h^s(\|\boldsymbol{I}_{\boldsymbol{\sigma}}\|_{D_h} + \|\boldsymbol{\varepsilon}_{\boldsymbol{\sigma}}\|_{D_h})\|\boldsymbol{U}\|_{D_h}. \tag{52}$$

Combining (51) and (52) with (48), we get

$$\begin{aligned}
(\boldsymbol{\varepsilon}_{\boldsymbol{V}}, \boldsymbol{U})_{D_h} \lesssim& h^s(\|\boldsymbol{I}_{\boldsymbol{\sigma}}\|_{D_h} + \|\boldsymbol{\varepsilon}_{\boldsymbol{\sigma}}\|_{D_h})\|\boldsymbol{U}\|_{D_h} \\
&+ h^{n/2+\delta/2-1/2}\|l^{-1/2}(\boldsymbol{g}^D - \boldsymbol{g}_h^D)\|_{\Gamma_h^D}\|\boldsymbol{U}\|_{D_h} + \|(G - G_h)\boldsymbol{n}\circ\boldsymbol{\phi}\|_{\Gamma_h^N}\|\boldsymbol{U}\|_{D_h}.
\end{aligned}$$

Then,

$$(\boldsymbol{\varepsilon_V},\boldsymbol{U})_{D_h} \lesssim (h^s + h^{n/2+\delta/2-1/2})(\|\boldsymbol{I_\sigma}\|_{D_h} + \|\boldsymbol{\varepsilon_\sigma}\|_{D_h} + \|l^{-1/2}(\boldsymbol{g}^D - \boldsymbol{g}_h^D)\|_{\Gamma_h^D})\|\boldsymbol{U}\|_{D_h} + \|(G-G_h)\boldsymbol{n}\circ\boldsymbol{\phi}\|_{\Gamma_h^N}\|\boldsymbol{U}\|_{D_h}.$$

Setting $\boldsymbol{U} = \boldsymbol{\varepsilon_V}$ in D_h, using (39) and defining $H_{\boldsymbol{V}} := h^s + h^{n/2+\delta/2-1/2}$.

$$\|\boldsymbol{\varepsilon_V}\|_{D_h} \lesssim H_{\boldsymbol{V}}\|\boldsymbol{I_\sigma}\|_{D_h} + R^{1/2}H_{\boldsymbol{V}}\|\boldsymbol{I_\sigma}\boldsymbol{n}_h\|_{\Gamma_h^D,h^\perp} + H_{\boldsymbol{V}}\left\|\left(h^{-1/2}\tfrac{\epsilon}{2} + \tau^{-1/2}\right)(G-G_h)\boldsymbol{n}\circ\boldsymbol{\phi}\right\|_{\Gamma_h^N} + H_{\boldsymbol{V}}R\|\partial_{\boldsymbol{n}_h}(\boldsymbol{I_\sigma}\boldsymbol{n}_h)\|_{D_h^c,(h^\perp)^2} + H_{\boldsymbol{V}}\|\tfrac{1}{2\epsilon}C_{tr}\boldsymbol{\varepsilon_V}\|_{D_h} + \|(G-G_h)\boldsymbol{n}\circ\boldsymbol{\phi}\|_{\Gamma_h^N}.$$

In addition, considering that $R \lesssim h^{n+\delta}$ (cf. (13)), we deduce that there exists a constant $C>0$, independent of h, such that

$$\|\boldsymbol{\varepsilon_V}\|_{D_h} \leq C\Bigg(H_{\boldsymbol{V}}\|\boldsymbol{I_\sigma}\|_{D_h} + h^{n/2+\delta/2}H_{\boldsymbol{V}}\|\boldsymbol{I_\sigma}\boldsymbol{n}_h\|_{\Gamma_h^D,h^\perp} + H_{\boldsymbol{V}}\left\|\left(h^{-1/2}\tfrac{\epsilon}{2} + \tau^{-1/2}\right)(G-G_h)\boldsymbol{n}\circ\boldsymbol{\phi}\right\|_{\Gamma_h^N} + h^{n+\delta}H_{\boldsymbol{V}}\|\partial_{\boldsymbol{n}_h}(\boldsymbol{I_\sigma}\boldsymbol{n}_h)\|_{D_h^c,(h^\perp)^2} + H_{\boldsymbol{V}}\|\tfrac{1}{2\epsilon}C_{tr}\boldsymbol{\varepsilon_V}\|_{D_h} + \|(G-G_h)\boldsymbol{n}\circ\boldsymbol{\phi}\|_{\Gamma_h^N}\Bigg).$$

Finally, choosing $\epsilon = CC_{tr}H_{\boldsymbol{V}}$, we have

$$\|\boldsymbol{\varepsilon_V}\|_{D_h} \lesssim H_{\boldsymbol{V}}\|\boldsymbol{I_\sigma}\|_{D_h} + h^{n/2+\delta/2}H_{\boldsymbol{V}}\|\boldsymbol{I_\sigma}\boldsymbol{n}_h\|_{\Gamma_h^D,h^\perp} + H_{\boldsymbol{V}}(H_{\boldsymbol{V}}h^{-1/2}+1)\|(G-G_h)\boldsymbol{n}\circ\boldsymbol{\phi}\|_{\Gamma_h^N} + \|(G-G_h)\boldsymbol{n}\circ\boldsymbol{\phi}\|_{\Gamma_h^N} + h^{n+\delta}H_{\boldsymbol{V}}\|\partial_{\boldsymbol{n}_h}(\boldsymbol{I_\sigma}\boldsymbol{n}_h)\|_{D_h^c,(h^\perp)^2},$$

and (50) after noticing that $s \geq 0$ and $n/2+\delta/2-1/2 \geq 0$. □

From the above lemma we can state the following theorem which gives us the convergence rates of the approximations.

Theorem 5.8. *Let us assume that $\boldsymbol{V} \in [H^{k+1}(\Omega)]^d$ and $\boldsymbol{\sigma} \in [H^{k+1}(\Omega)]^{d\times d}$. If the local proximity condition (13) is satisfied for $n \geq 1$ and $0<\delta<1$ and $s \geq 0$ in (47), then*

$$\|\boldsymbol{\varepsilon_V}\|_{D_h} \lesssim h^{k+1}H_{\boldsymbol{V}} + C_G h^{k+1/2}(H_{\boldsymbol{V}}^2 h^{-1/2}+1), \tag{53a}$$

$$\|\boldsymbol{\varepsilon_\sigma}\|_{D_h} \lesssim h^{k+1} + C_G h^k + \|\boldsymbol{\varepsilon_V}\|_{D_h}, \tag{53b}$$

and

$$\|\boldsymbol{V}-\boldsymbol{V}_h\|_\Omega \lesssim h^{k+1} + \|\boldsymbol{\varepsilon_V}\|_{D_h}, \quad \|\boldsymbol{\sigma}-\boldsymbol{\sigma}_h\|_\Omega \lesssim h^{k+1} + C_G h^k + \|\boldsymbol{\varepsilon_V}\|_{D_h}. \tag{53c}$$

Here, we recall that where $H_{\boldsymbol{V}} := h^s + h^{n/2+\delta/2-1/2}$.

Proof. By (64a), [24, Lemma 3.8] and (65), we note that

$$H_{\boldsymbol{V}}\|\boldsymbol{I_\sigma}\|_{D_h} + h^{n+\delta}H_{\boldsymbol{V}}\|\partial_{\boldsymbol{n}_h}(\boldsymbol{I_\sigma}\boldsymbol{n}_h)\|_{D_h^c,(h^\perp)^2} + h^{n/2+\delta/2}H_{\boldsymbol{V}}\|\boldsymbol{I_\sigma}\boldsymbol{n}_h\|_{\Gamma_h^D,h^\perp} \lesssim H_{\boldsymbol{V}}h^{k+1}.$$

In turn, by Lemma 5.5, we can deduce that

$$(H_{\boldsymbol{V}}^2h^{-1/2}+1)\|(G-G_h)\boldsymbol{n}\circ\boldsymbol{\phi}\|_{\Gamma_h^N} \lesssim C_G h^{k+1/2}(H_{\boldsymbol{V}}^2h^{-1/2}+1).$$

Therefore, combining all the above estimates, we prove (53a). On the other hand, choosing $\epsilon = 1$ in (39), we can deduce

$$\|\boldsymbol{\varepsilon_\sigma}\|_{D_h} \lesssim \|\boldsymbol{I_\sigma}\|_{D_h} + h^{n/2+\delta/2}\|\boldsymbol{I_\sigma}\|_{\Gamma_h^D,h^\perp} + \|h^{-1/2}(G-G_h)\boldsymbol{n}\circ\boldsymbol{\phi}\|_{\Gamma_h^N} + h^{n+\delta}\|\partial_{\boldsymbol{n}_h}(\boldsymbol{I_\sigma}\boldsymbol{n}_h)\|_{D_h^c,(h^\perp)^2} + \|\boldsymbol{\varepsilon_V}\|_{D_h}.$$

Then, by following steps analogous to those used to derive (53a), combining them with the estimate in Lemma 5.5 and bounding $\|\boldsymbol{\varepsilon_V}\|_{D_h}$ by (53a), we obtain (53b). Now, note that

$$\|\boldsymbol{V}-\boldsymbol{V}_h\|_\Omega \leq \|\boldsymbol{V}-\boldsymbol{V}_h\|_{D_h} + \|\boldsymbol{V}-\boldsymbol{V}_h\|_{D_h^c} \leq \|\boldsymbol{I_V}\|_{D_h} + \|\boldsymbol{\varepsilon_V}\|_{D_h} + \|\boldsymbol{V}-\boldsymbol{V}_h\|_{D_h^c}.$$

Then, applying [24, Lemma 3.7], we get

$$\|\boldsymbol{V}-\boldsymbol{V}_h\|_\Omega \leq \|\boldsymbol{I}_{\boldsymbol{V}}\|_{D_h} + \|\boldsymbol{\varepsilon}_{\boldsymbol{V}}\|_{D_h} + h\|\boldsymbol{I}_{\boldsymbol{\sigma}}\|_{D_h^c} + h^{\delta/2+1}\|\boldsymbol{\varepsilon}_{\boldsymbol{V}}\|_{D_h},$$

which implies the first estimate of (53c).

From [24, Lemma 3.8] we have that $\|\boldsymbol{I}_{\boldsymbol{\sigma}}\|_{D_h^c} \lesssim h^{k+1}$. In turn, By (64a) and (53a), we find that the first estimate of (53c) holds. On the other hand, analogue as above, we have

$$\|\boldsymbol{\sigma}-\boldsymbol{\sigma}_h\|_\Omega \leq \|\boldsymbol{I}_{\boldsymbol{\sigma}}\|_{D_h} + \|\boldsymbol{\varepsilon}_{\boldsymbol{\sigma}}\|_{D_h} + \|\boldsymbol{\sigma}-\boldsymbol{\sigma}_h\|_{D_h^c}\,.$$

By [24, Lemma 3.7], we get

$$\|\boldsymbol{\sigma}-\boldsymbol{\sigma}_h\|_\Omega \leq \|\boldsymbol{I}_{\boldsymbol{\sigma}}\|_{D_h} + \|\boldsymbol{\varepsilon}_{\boldsymbol{\sigma}}\|_{D_h} + \|\boldsymbol{I}_{\boldsymbol{\sigma}}\|_{D_h^c} + h^{\delta/2}\|\boldsymbol{\varepsilon}_{\boldsymbol{\sigma}}\|_{D_h}\,.$$

Finally, applying (64a), (53b), and [24, Lemma 3.8], then the second estimate of (53c) holds. □

6 Numerical experiments

We consider two numerical examples in two dimensions and set the stabilization parameter equal to one in all of them. The first one consists of a manufactured solution in a fixed domain, with the aim to compute errors and order of convergence of the schemes, while the second is intended to observe how a domain evolves when minimizing the energy functional.

6.1 Computational grids

The domain $\mathcal{M}$ is triangulated by a family (background triangulation) $\{T_h\}_{h>0}$ that satisfies the first three properties in the definition of *admissible triangulation* from Section 3. This ensures that the computational grids $\{\mathcal{T}_h\}_{h>0}$ obtained through (11) also satisfy these three conditions, as we can observe in Fig. 3. Regarding the fourth condition, computations require only that the mapping (12) is bijective at the vertices and the quadrature points of boundary edges. This—along with condition 4(a)—can be guaranteed by constructing the transfer paths according to the algorithm in [29, Section 2.4]. Said algorithm also provides the local proximity condition (13) with $n=1$ and $\delta=0$. In practice, numerical experiments show that the method performs optimally by picking the computational mesh from a family of background triangulations satisfying only these conditions.

6.2 Experiment 1: Convergence of the HDG scheme

In order to verify the orders of convergence of the HDG solvers, we consider a fixed domain

$$\Omega := \{x=(x_1,x_2)\in\mathbb{R}^2 : (0.05)^2 \leq |\boldsymbol{x}|^2 < (0.2)^2\},$$

the target function $\widetilde{y}(x_1,x_2) = -\sin(x_1)\sin(x_2)$ and $a=1$. The data f and g, and a non-homogeneous boundary condition in (5) are chosen such that $y(x_1,x_2)=\sin(x_1)\sin(x_2)$ is the solution to (2) and $z(x_1,x_2)=\sin(x_1)\sin(x_2)$ is the solution to (5), leading to $G(\Gamma)=0$. Then, to test the HDG approximation to the deformation field, we consider artificial right-hand sides in (6) so that $\boldsymbol{V}(x_1,x_2) = e^{|\boldsymbol{x}|^2-0.05^2}(1,1)^t$ is the solution to (6).

Numerical experiments for polynomial bases of degrees $k=1,2,3$ were performed and the convergence history of the scheme, as a function of the number of mesh elements N, is shown in Figure 2. As a reference, the black dashed line indicates the slope h^{k+1}, which coincides with the experimental order of convergence, in the L^2–norm, of the volume variables (plotted in blue and red lines in the figure). This behavior is better than the one predicted by Theorem 5.8 which, for $n=1$ and $\delta=0$ as in our case, predicts that the order of convergence for all the errors is h^k. Note that the error in the traces (plotted in yellow) measured with respect to the norm

$$|||\cdot|||_h := \left(\sum_{K\in D_h} h_K\|\cdot\|^2_{\partial K}\right)^{1/2},$$

superconverges with order h^{k+2} as proven for Dirichlet boundary value problems in [24, 29].

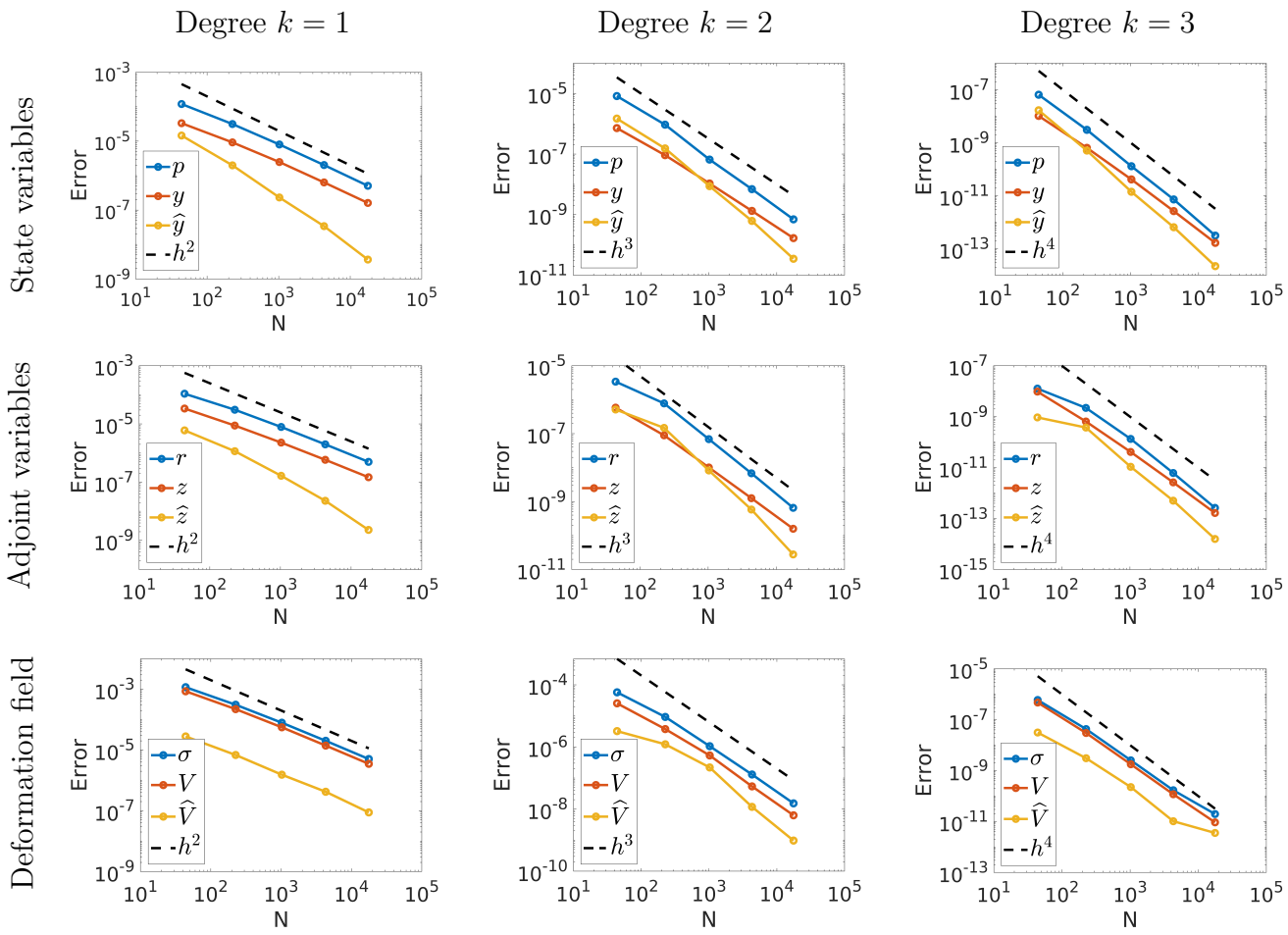

Figure 2: Convergence history for the variables associated to the three systems— state, adjoint and deformation— for different orders of polynomial bases. The trace variables (denoted with a "hat $\widehat{\cdot}$" and plotted in yellow) all converge with an additional power of h.

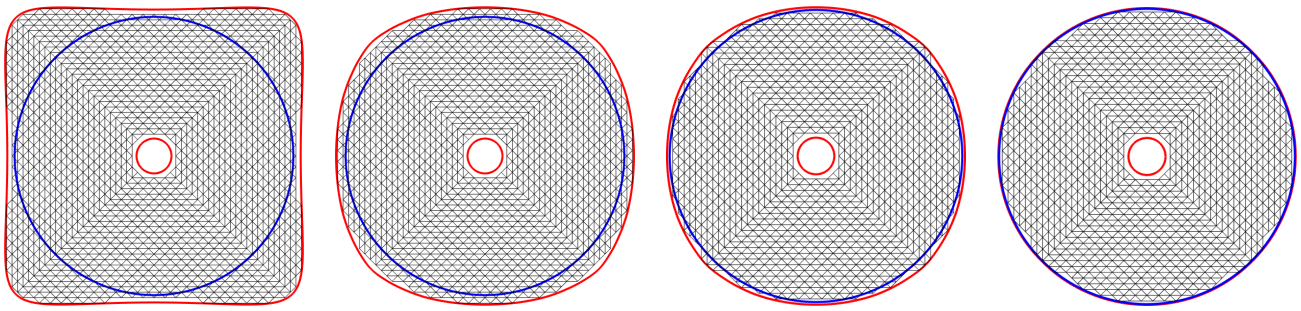

Figure 3: Numerical approximation to the optimal shape for iterations: 0, 30, 50, 90. The optimal shape is drawn in blue, while the numerical approximation is drawn in red. The computational mesh used for solving the state, adjoint and deformation equations is plotted in black. After 90 iterations the two curves are indistinguishable to the naked eye.

6.3 Experiment 2: Shape optimization with a manufactured example.

Consider the target function

$$\widetilde{y}(x_1, x_2) := \left(|\boldsymbol{x}|^2 - \frac{1}{2\pi}\right)\left(|\boldsymbol{x}|^2 - 0.05^2\right),$$

along with the problem data

$$f(x_1, x_2) = \left(4|\boldsymbol{x}|^2 - \frac{1}{2\pi} - 0.05^2\right), \qquad g = 0\,, \qquad \text{and} \qquad a = 1.$$

With these parameters, the solution to the state equation (2) is $y(x_1, x_2) = \frac{1}{4}\,\widetilde{y}(x_1, x_2)$.

Let $\mathcal{U} := \{\boldsymbol{x} = (x_1, x_2) \in (-1, 1)^2 : |\boldsymbol{x}| > 0.05\}$ and consider the set of admissible domains

$$\mathcal{O} := \left\{\Omega : \Omega \subset \mathcal{U} \;\text{ and }\; \mu(\Omega) = m_0 := \pi\left(\frac{1}{2\pi} - 0.05^2\right) \text{ with } \{|\boldsymbol{x}| = 0.05\} \subset \partial\Omega\right\}.$$

In this case, we expect the optimal domain to be

$$\widehat{\Omega} = \left\{\boldsymbol{x} = (x_1, x_2) \in \mathcal{U} : |\boldsymbol{x}|^2 < \frac{1}{2\pi}\right\},$$

and the optimal energy to be given by

$$J(\widehat{\Omega}; y) = \frac{9}{8}\int_{\widehat{\Omega}} \widetilde{y}^2(x_1, x_2)\; d(x_1, x_2) = \frac{9\pi}{16}\int_{0.05}^{1/\sqrt{2\pi}} r\left(r^2 - \frac{1}{2\pi}\right)^2 (r^2 - 0.05^2)^2\, dr \approx 6.83 \times 10^{-8}.$$

Algorithm 2 was employed using the value $\epsilon = 10^{-4}$ (see eq. (10)) and starting from the initial guess for Ω displayed in red on the leftmost panel of Figure 3. To enforce the condition that $|\boldsymbol{x}| = 0.05$ remains a subset of $\partial\Omega$, the initial guess includes this segment in its boundary and the Dirichlet condition $\boldsymbol{V} = 0$ on $\{|\boldsymbol{x}| = 0.05\}$ is included in the BVP for the deformation field. The initial guess for the domain Ω consisted of a sample of $N = 2000$ points p_i not located on the fixed inner circle $\{|\boldsymbol{x} = 0.05|\}$. These points were iteratively displaced according to the deformation field as $p_i \mapsto p_i + \tau \boldsymbol{V}(p_i)$, where the value of τ is updated in every step through an Armijo line search.

This results in a polygonal approximation of the optimal boundary. As the shape of the approximated domain changes, the computational mesh (displayed in black on Figure 3) is updated. The approximation after 90 iterations is displayed on the rightmost panel in Figure 3. The maximum length of a segment in our final polygonal approximation is $\ell = 1.8 \times 10^{-3}$. Using a traditional approach reliant on an interpolatory uniform mesh, where the number of elements is proportional to h^{-2}, such a resolution would require approximately 3×10^5 elements compared to the 1924 elements in our grid. This dramatic reduction (a factor of approximately 1.5×10^2) on the number of elements required underscores the efficiency of the proposed technique.

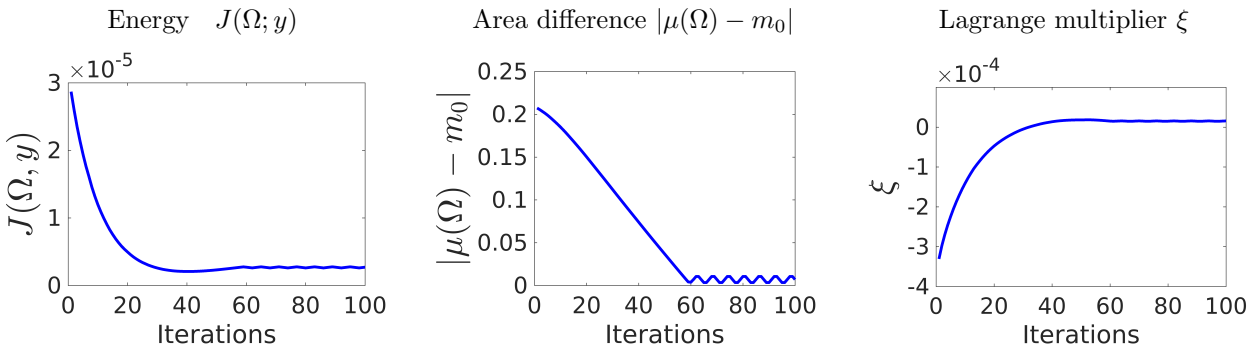

Figure 4: Left: The target energy functional $J(\Omega; y)$ decreases as the number of iterations grows, settling after about 50 iterations. Center: The violation of the area constraint decreases steadily and reaches a steady state after about 60 iterations. Right: The value of the Lagrange multiplier grows with the number of iterations, switching from assigning more importance to the shape of the domain at the beginning, towards enforcement of the area constraint at the end.

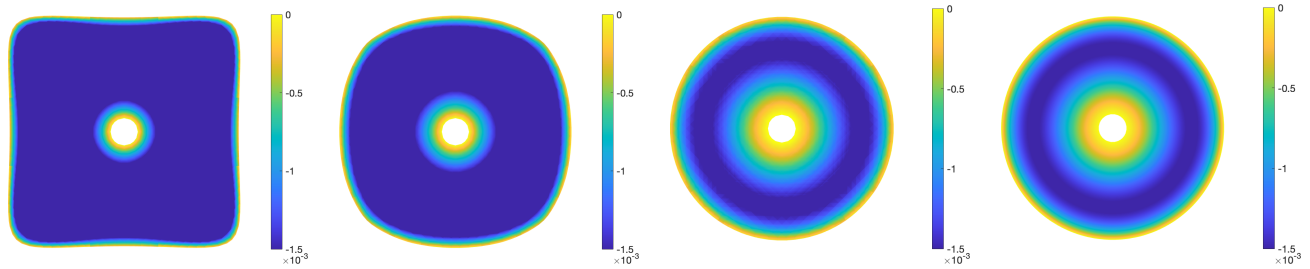

Initial guess for y | y after 30 iterations | y after 90 iterations | Optimal y

Figure 5: The three panels on the left depict the evolution of the state variable from the initial guess until 90 iterations. The rightmost panel shows the optimal state, which equals $\widetilde{y}/4$.

The value of the Lagrange multiplier is updated according to equation (10). As shown in the right panel of Figure 4, initially the value of the Lagrange multiplier ξ is small, penalizing mostly the energy term $J(\Omega; y)$ that determines the shape of the domain. As the algorithm progresses, the value of ξ increases, penalizing mostly the violation of the volume constraint. Accordingly, the value of the energy decreases sharply at the beginning (left panel of Figure 4 and increases a little before settling down, while the value of the area difference decreases steadily until it oscillates around a steady value (center panel of Figure 4). The slight increase in the energy towards the end of the process reflects the fact that a more energetically efficient shape can be obtained (similar to the red curve in the center–left panel of Figure 3) if the volume constraint is dropped. The evolution of the state variable y as the shape of the domain changes is depicted in Figure 5.

7 Concluding remarks

This article was mostly devoted to the analysis of the unfitted HDG discretizations associated to the state, adjoint and deformation problems arising from a model problem in geometric shape optimization. The analysis faces the, now well–known, challenges associated to a Neumann type boundary condition stemming from condition (27c) in the problem for the deformation field. The challenge manifests itself in the error bounds for $\boldsymbol{V}$ through the appearance of the term $\|(G - G_h)\boldsymbol{n} \circ \boldsymbol{\phi}\|_{\Gamma_h^N}$, whose optimal bound remains elusive. Nevertheless, numerical experiments (as is the case of Experiment 1) repeatedly show that the optimal order may be feasible, even in the when employing triangulations that are not fully admissible in the sense defined in Section 3. Ensuring these bounds theoretically remains an open challenge.

However, an interesting and promising path arises from the findings of the second numerical experiment. The fact that the transfer path technique enables a very accurate and efficient description of the optimal boundary. Efficiency in this context refers to the fact that the maximum length of the sides of the polygonal approximation can be made at least as small as h^2 for a regular mesh of diameter h. This feature has the potential of speeding up computations

by several orders of magnitude and, very importantly, is independent of the method chosen for the discretization of the associated boundary value problems, as long as they are cast in a mixed form. Due to the fact that this feature is independent of HDG, its analysis and further explorations are the subject of ongoing work and will be shared in a separate communication [37].

8 Acknowledgements

Esteban Henríquez and Manuel E. Solano were partially supported by ANID-Chile through Basal Project FB210005 and Fondecyt 1240183. Tonatiuh Sánchez-Vizuet was partially supported by the United States National Science Foundation through the grant NSF-DMS-2137305 "LEAPS-MPS: Hybridizable discontinuous Galerkin methods for non-linear integro-differential boundary value problems in magnetic plasma confinement".

A Auxiliary estimates

For any $e \in \mathcal{E}_h^\partial$, any point $\boldsymbol{x}$ lying on the face e and any smooth enough function $\boldsymbol{v}$ defined in K_e^{ext}, we set

$$\Lambda^{\boldsymbol{v}}(\boldsymbol{x}) := \frac{1}{l(\boldsymbol{x})} \int_0^{l(\boldsymbol{x})} (\boldsymbol{v}(\boldsymbol{x} + s\,\boldsymbol{n}_h) - \boldsymbol{v}(\boldsymbol{x})) \cdot \boldsymbol{n}_h \, ds\,. \tag{54}$$

For each $e \in \mathcal{E}_h^\partial$, and vector–valued functions $\boldsymbol{v}$ and $\boldsymbol{n}_h$ such that their scalar product $\boldsymbol{v} \cdot \boldsymbol{u}_h \in H^1(K_e^{ext})$, it satisfies (cf. [24, Lemma 5.2])

$$\|\Lambda^{\boldsymbol{v}}\|_{e,l} \le \frac{1}{\sqrt{3}}\, r_e\, \|\partial_{\boldsymbol{n}_h}(\boldsymbol{v}\cdot\boldsymbol{n}_h)\|_{K_e^{ext},(h^\perp)^2}\,, \tag{55}$$

where we have used the notation $\partial_{\boldsymbol{n}_h} u := \nabla u \cdot \boldsymbol{n}_h$. Moreover, if $\boldsymbol{v} \in [\mathbb{P}_k(K_e)]^d$, we have that

$$\|\Lambda^{\boldsymbol{v}}\|_{e,l} \le \frac{1}{\sqrt{3}}\, r_e^{3/2}\, C_e^{ext}\, C_e^{inv}\, \|\boldsymbol{v}\|_{K_e}\,. \tag{56}$$

We also recall the discrete trace inequality, whose proof can be found in [31, Lemma 1.52], for instance. Let K be an element of $\mathcal{T}_h$ with diameter h and $v \in \mathbb{P}_k(K)$. Then there exists $C_{tr} > 0$, depending only on k and mesh regularity, such that

$$h^{1/2}\, \|v\|_e \le C_{tr}\, \|v\|_K\,, \tag{57}$$

where e is a edge or face of K.

The following estimates are used in Section 5.1 to find estimates for the term $\|(G - G_h)\boldsymbol{n}\circ\boldsymbol{\phi}\|_{\Gamma_h^N}$.

Lemma A.1. *For a polynomial p defined over a boundary element K_e associated with the edge e and the extension patch K_e^{ext}, and for all $v \in H^1(K_e)$ the following estimates hold*

$$h_e^{1/2}\, \|p\|_{\Gamma_e} \lesssim \|p\|_{K_e^{ext}\cup K_e}, \tag{58}$$

$$h_e^{1/2}\, \|v\|_{\Gamma_e} \lesssim \left(\|v\|^2_{K_e^{ext}\cup K_e} + h_e^2\, \|\nabla v\|^2_{K_e^{ext}\cup K_e}\right)^{1/2}. \tag{59}$$

Proof. Let us define the following reference patch

$$\widehat{K} := \{\widehat{\boldsymbol{y}} :\ \widehat{\boldsymbol{y}} = \boldsymbol{y}/(H_e + h_e)\,,\ \boldsymbol{y} \in K_e^{ext}\cup K_e\}\,.$$

Additionally, we define $\widehat{p}(\widehat{\boldsymbol{y}}) := p(\boldsymbol{y}/H_e)$ and $\widehat{\Gamma}_e$ denotes the part of the boundary of $\widehat{K}_e^{ext}$ that has been mapped form Γ_e. Then, applying trace inequality in the reference patch $\widehat{K}_e^{ext}$, we have

$$\|p\|^2_{\Gamma_e} \lesssim |\Gamma_e|\|\widehat{p}\|^2_{\widehat{\Gamma}_e} \lesssim |\Gamma_e|\|\widehat{p}\|^2_{\widehat{K}} \lesssim |\Gamma_e||K_e^{ext}\cup K_e|^{-1}\|p\|^2_{K_e^{ext}\cup K_e} \lesssim h_e^{-1}\|p\|^2_{K_e^{ext}\cup K_e} \qquad \forall p \in \mathbb{P}_k(K_e^{ext}\cup K_e)\,,$$

where we note that $|\Gamma_e|$ is proportional to h_e and $|K_e^{ext}\cup K_e|$ is proportional to h_e^2, and then (58) holds. Next, (59) holds following similar steps to ones above, but using the continuous trace inequality on the reference patch. □

Lemma A.2. *If B_e is a ball with center at the middle point of e, such that $K_e^{ext} \cup K_e \subset B_e$, and for all $m \in \mathbb{Z}_0^+$,*

$$\boldsymbol{E} : \boldsymbol{H}^{m+1}(\Omega) \to \boldsymbol{H}^{m+1}(\mathbb{R}^d)$$

is an extension operator such that

$$\boldsymbol{E}(\boldsymbol{\rho})|_\Omega = \boldsymbol{\rho} \quad \text{for all } \boldsymbol{\rho} \in \boldsymbol{H}^{m+1}(\Omega) \qquad \text{and} \qquad \|\boldsymbol{E}(\boldsymbol{\rho})\|_{\boldsymbol{H}^{m+1}(\mathbb{R}^d)} \lesssim \|\boldsymbol{\rho}\|_{\boldsymbol{H}^{m+1}(\Omega)}\,, \tag{60}$$

then

$$\|\boldsymbol{I}_{\boldsymbol{p}}\|_{K_e^{ext}} \lesssim (1 + r_e^{1/2})\, h_e^{m+1}\, |\boldsymbol{E}(\boldsymbol{p})|_{\boldsymbol{H}^{m+1}(B_e)} + r_e^{1/2}\, \|\boldsymbol{I}_{\boldsymbol{p}}\|_{K_e}\,, \tag{61}$$

$$\|\nabla \boldsymbol{I}_{\boldsymbol{p}}\|_{K_e^{ext}} \lesssim h^m\, |\boldsymbol{E}(\boldsymbol{p})|_{\boldsymbol{H}^{m+1}(B_e)} + r_e^{1/2}\, h_e^m\, \|\boldsymbol{E}(\boldsymbol{p})\|_{\boldsymbol{H}^{m+1}(K_e)} + r_e^{1/2}\, h_e^{-1}\, \|\boldsymbol{I}_{\boldsymbol{p}}\|_{K_e}\,. \tag{62}$$

For the proof of this Lemma we refer to [11, Lemma 3].

B HDG–projections and their properties

For the error analysis we will use an extension of the HDG–projection developed in [22] for matrix/vector valued functions. For $(\boldsymbol{\sigma}, \boldsymbol{w}) \in \mathbb{Z}_h \times \boldsymbol{W}_h$ we define $\Pi_h(\boldsymbol{\sigma}, \boldsymbol{w}) := (\boldsymbol{\Pi}_{\mathbb{Z}}\boldsymbol{\sigma}, \boldsymbol{\Pi}_{\boldsymbol{W}}\boldsymbol{w})$ to be the unique solutions of the system

$$(\boldsymbol{\Pi}_{\mathbb{Z}}\boldsymbol{\sigma}, \boldsymbol{s})_K = (\boldsymbol{r}, \boldsymbol{s})_K \qquad \forall\, \boldsymbol{s} \in [\mathbb{P}_{k-1}(K)]^{d\times d}\,, \tag{63a}$$

$$(\Pi_{\boldsymbol{W}}\boldsymbol{w}, \boldsymbol{v})_K = (\boldsymbol{w}, \boldsymbol{v})_K \qquad \forall\, \boldsymbol{v} \in [\mathbb{P}_{k-1}(K)]^{d}\,, \tag{63b}$$

$$\langle \boldsymbol{\Pi}_{\mathbb{Z}}\boldsymbol{\sigma}\boldsymbol{n} + \tau\, \Pi_{\boldsymbol{W}}\boldsymbol{w}, \boldsymbol{\mu}\rangle_e = \langle \boldsymbol{\sigma}\boldsymbol{n} + \tau\, \boldsymbol{w}, \boldsymbol{\mu}\rangle_e \qquad \forall\, \boldsymbol{\mu} \in [\mathbb{P}_k(e)]^d, \ \text{ and } \forall\, e \subset \partial K\,. \tag{63c}$$

As proven in [22, Theorem 2.1], the HDG–projection is well–defined and satisfies the following properties:

- If $\boldsymbol{r} \in \boldsymbol{H}^{k+1}(K)$ and $w \in H^{k+1}(K)$,

$$\|\boldsymbol{\Pi}_{\boldsymbol{Z}}\boldsymbol{r} - \boldsymbol{r}\|_K \lesssim h_K^{k+1}\, |\boldsymbol{r}|_{\boldsymbol{H}^{k+1}(K)} + h_K^{k+1}\, \tau\, |w|_{H^{k+1}(K)}\,, \tag{64a}$$

$$\|\Pi_W w - w\|_K \lesssim h_K^{k+1}\, |w|_{H^{k+1}(K)} + \frac{h_K^{k+1}}{\tau}\, |\nabla\cdot \boldsymbol{r}|_{H^k(K)}\,. \tag{64b}$$

- If e is an edge or face of Γ_h then (cf. [24])

$$\|(\boldsymbol{\Pi}_{\boldsymbol{Z}}\boldsymbol{r} - \boldsymbol{r})\, \boldsymbol{n}_h\|_{\Gamma_h, h^\perp} \lesssim h^{k+1}\, |\boldsymbol{r}|_{\boldsymbol{H}^{k+1}(\Omega)} + h^{k+1}\, \tau\, |w|_{H^{k+1}(\Omega)}\,, \tag{65}$$

  where the weighted norm $\|\cdot\|_{\Gamma_h, h^\perp}$ is as defined in (19).

We will also make use of the orthogonal L^2–projection over an element K of a function v, denoted by $P_{L^2(K)}v$. It is well known ([31, Lemmas 1.58 and 1.59]) that, if $v \in H^{l+1}(K)$ for $0 \le l \le k$,

$$|v - P_{L^2(K)}v|_{H^m(K)} \lesssim h^{l+1-m}\, |v|_{H^{l+1}(K)} \quad \forall m \in \{0, \dots, k\}\,, \tag{66a}$$

$$\|v - P_{L^2(K)}v\|_{\partial K} \lesssim h^{l+1/2}\, |v|_{H^{l+1}(K)}\,. \tag{66b}$$

We point out that the previous projection errors can be extended to the vector-valued case.

As final property we state the following estimate

Lemma B.1. *Let $\boldsymbol{r} \in \boldsymbol{H}^{k+1}(K)$ and $w \in H^{k+1}(K)$, then*

$$\|\nabla(\boldsymbol{\Pi}_{\boldsymbol{Z}}\boldsymbol{r} - \boldsymbol{r})\|_K \lesssim h_K^k \big(|\boldsymbol{r}|_{\boldsymbol{H}^{k+1}(K)} + |y|_{H^{k+1}(K)}\big)\,. \tag{67}$$

Proof. Note that

$$\|\nabla(\boldsymbol{\Pi}_{\boldsymbol{Z}}\boldsymbol{r} - \boldsymbol{r})\|_K \le \|\nabla(\boldsymbol{\Pi}_{\boldsymbol{Z}}\boldsymbol{p} - \boldsymbol{P}_{\boldsymbol{L}^2(K)}\boldsymbol{p})\|_K + \|\nabla(\boldsymbol{P}_{\boldsymbol{L}^2(K)}\boldsymbol{p} - \boldsymbol{p})\|_K.$$

Using and inverse inequality (see [31, Lemma 1.44]) in the first term and (66a) in the second term,

$$\|\nabla(\boldsymbol{\Pi}_{\boldsymbol{Z}}\boldsymbol{r} - \boldsymbol{r})\|_K \lesssim h_K^{-1}\|\boldsymbol{\Pi}_{\boldsymbol{Z}}\boldsymbol{p} - \boldsymbol{P}_{\boldsymbol{L}^2(K)}\boldsymbol{p}\|_K + h_K^k |\boldsymbol{p}|_{\boldsymbol{H}^{k+1}(K)} \le h_K^{-1}\|\boldsymbol{\Pi}_{\boldsymbol{Z}}\boldsymbol{p} - \boldsymbol{p}\|_K + h_K^{-1}\|\boldsymbol{p} - \boldsymbol{P}_{\boldsymbol{L}^2(K)}\boldsymbol{p}\|_K + h_K^k |\boldsymbol{p}|_{\boldsymbol{H}^{k+1}(K)}.$$

Finally, applying (64a) and (66a), we find that (67) holds. □

References

[1] G. Allaire, C. Dapogny, and P. Frey. Shape optimization with a level set based mesh evolution method. *Computer Methods in Applied Mechanics and Engineering*, 282:22–53, 2014.

[2] G. Allaire, F. Jouve, and A.-M. Toader. Structural optimization by the level-set method. In P. Colli, C. Verdi, and A. Visintin, editors, *Free Boundary Problems*, pages 1–15, Basel, 2004. Birkhäuser Basel.

[3] R. Araya, M. Solano, and P. Vega. A posteriori error analysis of an HDG method for the Oseen problem. *Applied Numerical Mathematics*, 146:291–308, 2019.

[4] F. Artaza-Covarrubias, T. Sánchez-Vizuet, and M. Solano. A coupled HDG discretization for the interaction between acoustic and elastic waves. *(Submitted)*, 2025. (arXiv: 2505.15106).

[5] L. L. Beghini, A. Beghini, N. Katz, W. F. Baker, and G. H. Paulino. Connecting architecture and engineering through structural topology optimization. *Engineering Structures*, 59:716–726, 2014.

[6] I. Bermúdez, J. Manríquez, and M. Solano. A hybridizable discontinuous Galerkin method for Stokes/Darcy coupling on dissimilar meshes. *IMA Journal of Numerical Analysis*, Apr. 2025.

[7] C. Bertsch, A. P. Cisilino, S. Langer, and S. Reese. Topology optimization of 3D elastic structures using boundary elements. In *PAMM: Proceedings in Applied Mathematics and Mechanics*, volume 8, pages 10771–10772. Wiley Online Library, 2008.

[8] B. Braida, J. Dalphin, C. Dapogny, P. Frey, and Y. Privat. Shape and topology optimization for maximum probability domains in quantum chemistry. *Numerische Mathematik*, pages 1–48, 2022.

[9] E. Burman, D. Elfverson, P. Hansbo, M. G. Larson, and K. Larsson. A cut finite element method for the Bernoulli free boundary value problem. *Computer Methods in Applied Mechanics and Engineering*, 317:598–618, 2017.

[10] E. Burman, D. Elfverson, P. Hansbo, M. G. Larson, and K. Larsson. Shape optimization using the cut finite element method. *Computer Methods in Applied Mechanics and Engineering*, 328:242–261, 2018.

[11] L. Camargo and M. Solano. A high order unfitted HDG method for the Helmholtz equation with first order absorbing boundary condition. *Preprint, Centro de Investigación en Ingeniería Matemática (CI^2MA)*, 27, 2021.

[12] E. Cancès, R. Keriven, F. Lodier, and A. Savin. How electrons guard the space: shape optimization with probability distribution criteria. *Theoretical Chemistry Accounts*, 111(2):373–380, 2004.

[13] J. Carrero, B. Cockburn, and D. Schötzau. Hybridized globally divergence-free LDG methods. Part I: The Stokes problem. *Mathematics of computation*, 75(254):533–563, 2006.

[14] A. Cesmelioglu, B. Cockburn, N. C. Nguyen, and J. Peraire. Analysis of HDG methods for Oseen equations. *Journal of Scientific Computing*, 55(2):392–431, 2013.

[15] A. Cesmelioglu, B. Cockburn, and W. Qiu. Analysis of a hybridizable discontinuous Galerkin method for the steady-state incompressible Navier-Stokes equations. *Mathematics of Computation*, 86(306):1643–1670, 2017.

[16] V. J. Challis and J. K. Guest. Level set topology optimization of fluids in Stokes flow. *International journal for numerical methods in engineering*, 79(10):1284–1308, 2009.

[17] Y. Chen and B. Cockburn. Analysis of variable-degree HDG methods for convection-diffusion equations. Part I: general nonconforming meshes. *IMA Journal of Numerical Analysis*, 32(4):1267–1293, Feb. 2012.

[18] Y. Chen and B. Cockburn. Analysis of variable-degree HDG methods for convection-diffusion equations. Part II: Semimatching nonconforming meshes. *Mathematics of Computation*, 83(285):87–111, May 2013.

[19] B. Cockburn, B. Dong, and J. Guzmán. A superconvergent LDG-hybridizable Galerkin method for second-order elliptic problems. *Mathematics of Computation*, 77(264):1887–1916, 2008.

[20] B. Cockburn, B. Dong, J. Guzmán, M. Restelli, and R. Sacco. A hybridizable discontinuous Galerkin method for steady-state convection-diffusion-reaction problems. *SIAM Journal on Scientific Computing*, 31(5):3827–3846, 2009.

[21] B. Cockburn, J. Gopalakrishnan, and R. Lazarov. Unified hybridization of discontinuous Galerkin, mixed, and continuous Galerkin methods for second order elliptic problems. *SIAM Journal on Numerical Analysis*, 47(2):1319–1365, 2009.

[22] B. Cockburn, J. Gopalakrishnan, and F.-J. Sayas. A projection-based error analysis of HDG methods. *Mathematics of Computation*, 79(271):1351–1367, Mar. 2010.

[23] B. Cockburn, J. Guzmán, and H. Wang. Superconvergent discontinuous Galerkin methods for second-order elliptic problems. *Mathematics of Computation*, 78(265):1–24, 2009.

[24] B. Cockburn, W. Qiu, and M. Solano. A priori error analysis for HDG methods using extensions from subdomains to achieve boundary conformity. *Mathematics of computation*, 83(286):665–699, 2014.

[25] B. Cockburn and V. Quenneville-Bélair. Uniform-in-time superconvergence of the HDG methods for the acoustic wave equation. *Mathematics of Computation*, 83(285):65–85, 2014.

[26] B. Cockburn, F.-J. Sayas, and M. Solano. Coupling at a distance HDG and BEM. *SIAM Journal on Scientific Computing*, 34(1):A28–A47, 2012.

[27] B. Cockburn and K. Shi. Conditions for superconvergence of HDG methods for Stokes flow. *Mathematics of Computation*, 82(282):651–671, 2013.

[28] B. Cockburn and K. Shi. Superconvergent HDG methods for linear elasticity with weakly symmetric stresses. *IMA Journal of Numerical Analysis*, 33(3):747–770, 2013.

[29] B. Cockburn and M. Solano. Solving Dirichlet boundary-value problems on curved domains by extensions from subdomains. *SIAM Journal on Scientific Computing*, 34(1):A497–A519, 2012.

[30] B. Cockburn and M. Solano. Solving convection-diffusion problems on curved domains by extensions from subdomains. *Journal of Scientific Computing*, 59(2):512–543, 2014.

[31] D. A. Di Pietro and A. Ern. *Mathematical aspects of discontinuous Galerkin methods*, volume 69. Springer Science & Business Media, 2011.

[32] G. Dogan, P. Morin, R. H. Nochetto, and M. Verani. Discrete gradient flows for shape optimization and applications. *Computer methods in applied mechanics and engineering*, 196(37-40):3898–3914, 2007.

[33] X.-B. Duan, Y.-C. Ma, and R. Zhang. Shape-topology optimization of Stokes flow via variational level set method. *Applied Mathematics and Computation*, 202(1):200–209, 2008.

[34] G. Fu, W. Qiu, and W. Zhang. An analysis of HDG methods for convection-dominated diffusion problems. *ESAIM: Mathematical Modelling and Numerical Analysis*, 49(1):225–256, 2015.

[35] G. N. Gatica and F. A. Sequeira. A priori and a posteriori error analyses of an augmented HDG method for a class of quasi-Newtonian Stokes flows. *Journal of Scientific Computing*, 69(3):1192–1250, 2016.

[36] L. F. Gatica and F. A. Sequeira. A priori and a posteriori error analyses of an HDG method for the Brinkman problem. *Computers & Mathematics with Applications*, 75(4):1191–1212, 2018.

[37] E. Henríquez, T. Sánchez-Vizuet, and M. Solano. The transfer path method for unfitted discretizations in shape optimization. *In preparation*, 2025.

[38] E. Henríquez and M. Solano. An unfitted HDG method for a distributed optimal control problem. *Journal of Computational and Applied Mathematics*, 441:115703, 2024.

[39] A. Henrot and J. Sokołowski. Mathematical challenges in shape optimization. *Control and Cybernetics*, 34(1):37–57, 2005.

[40] J. S. Jensen and O. Sigmund. Topology optimization for nano-photonics. *Laser & Photonics Reviews*, 5(2):308–321, 2011.

[41] R. M. Kirby, S. J. Sherwin, and B. Cockburn. To CG or to HDG: a comparative study. *Journal of Scientific Computing*, 51(1):183–212, 2012.

[42] N. Lebbe, C. Dapogny, E. Oudet, K. Hassan, and A. Gliere. Robust shape and topology optimization of nanophotonic devices using the level set method. *Journal of Computational Physics*, 395:710–746, 2019.

[43] J. Manríquez, N.-C. Nguyen, and M. Solano. A dissimilar non-matching HDG discretization for Stokes flows. *Computer Methods in Applied Mechanics and Engineering*, 399:115292, 2022.

[44] A. Manzoni, A. Quarteroni, and S. Salsa. *Optimal Control of Partial Differential Equations*. Springer, 2021.

[45] L. C. Neches and A. P. Cisilino. Topology optimization of 2D elastic structures using boundary elements. *Engineering analysis with boundary elements*, 32(7):533–544, 2008.

[46] N. C. Nguyen and J. Peraire. Hybridizable discontinuous Galerkin methods for partial differential equations in continuum mechanics. *Journal of Computational Physics*, 231(18):5955–5988, 2012.

[47] N. C. Nguyen, J. Peraire, and B. Cockburn. An implicit high-order hybridizable discontinuous Galerkin method for the incompressible Navier–Stokes equations. *Journal of Computational Physics*, 230(4):1147–1170, 2011.

[48] N. C. Nguyen, J. Peraire, and B. Cockburn. A class of embedded discontinuous Galerkin methods for computational fluid dynamics. *Journal of Computational Physics*, 302:674–692, 2015.

[49] W. Qiu, M. Solano, and P. Vega. A high order HDG method for curved-interface problems via approximations from straight triangulations. *Journal of Scientific Computing*, 69(3):1384–1407, 2016.

[50] W. H. Reed and T. R. Hill. Triangular mesh methods for the neutron transport equation. Technical report, Los Alamos Scientific Lab., N. Mex.(USA), 1973.

[51] S. Rhebergen, B. Cockburn, and J. J. Van Der Vegt. A space–time discontinuous Galerkin method for the incompressible Navier–Stokes equations. *Journal of computational physics*, 233:339–358, 2013.

[52] N. Sánchez, T. Sánchez-Vizuet, and M. Solano. Error analysis of an unfitted HDG method for a class of non-linear elliptic problems. *Journal of Scientific Computing*, 90(3), Feb. 2022.

[53] N. Sánchez, T. Sánchez-Vizuet, and M. E. Solano. A priori and a posteriori error analysis of an unfitted HDG method for semi-linear elliptic problems. *Numerische Mathematik*, 148(4):919–958, Aug. 2021.

[54] N. Sánchez, T. Sánchez-Vizuet, and M. E. Solano. Afternote to "Coupling at a distance": Convergence analysis and a priori error estimates. *Computational Methods in Applied Mathematics*, 22(4):945–970, July 2022.

[55] T. Sánchez-Vizuet and M. E. Solano. A hybridizable discontinuous Galerkin solver for the Grad-Shafranov equation. *Computer Physics Communications*, 235:120–132, Feb 2019.

[56] T. Sánchez-Vizuet, M. E. Solano, and A. J. Cerfon. Adaptive hybridizable discontinuous Galerkin discretization of the Grad–Shafranov equation by extension from polygonal subdomains. *Computer Physics Communications*, 255:107239, 2020.

[57] M. Solano and F. Vargas. A high order HDG method for Stokes flow in curved domains. *Journal of Scientific Computing*, 79(3):1505–1533, 2019.

[58] M. Solano and F. Vargas. An unfitted HDG method for Oseen equations. *Journal of Computational and Applied Mathematics*, 399:113721, 2022.

[59] S.-C. Soon, B. Cockburn, and H. K. Stolarski. A hybridizable discontinuous Galerkin method for linear elasticity. *International journal for numerical methods in engineering*, 80(8):1058–1092, 2009.

[60] S. Zhou and Q. Li. A variational level set method for the topology optimization of steady-state Navier–Stokes flow. *Journal of Computational Physics*, 227(24):10178–10195, 2008.

Centro de Investigación en Ingeniería Matemática (CI^{2}MA)

PRE-PUBLICACIONES 2025

2025-10 Veronica Anaya, Gerardo Chowell, Felipe Jara, Mauricio Sepúlveda: *Optimal control of inter-population disease spread via reaction–diffusion models*

2025-11 Ramiro Acevedo, Rommel Bustinza, Christian Gómez: *A transient Eddy current problem via potential formulation with current excitation*

2025-12 Abraham J. Arenas, Juan Barajas-Calonge, Gilberto González-Parra, Luis M. Villada: *A second-order nonstandard finite difference scheme for eco-epidemiological predator-prey models*

2025-13 Alonso J. Bustos, Sergio Caucao, Gabriel N. Gatica: *Mixed-primal and fully-mixed formulations for the convection-diffusion-reaction system based upon Brinkman–Forchheimer equations*

2025-14 Gabriel N. Gatica, Zeinab Gharibi, Ricardo Oyarzúa: *Banach spaces-based fully mixed finite element methods for the n-dimensional Boussinesq problem with temperature-dependent parameters*

2025-15 Sergio Caucao, Ricardo Oyarzúa, Segundo Villa-Fuentes: *A priori and a posteriori error analyses of a fully-mixed finite element method for the coupled Navier Stokes / Darcy problem*

2025-16 Juan Barajas-Calonge, Raimund Bürger, Pep Mulet, Luis M. Villada: *A second-order invariant-region-preserving scheme for a transport-flow model of polydisperse sedimentation*

2025-17 Raimund Bürger, Stefan Diehl, María Carmen Martí, Yolanda Vásquez: *A numerical scheme for a model of a flotation column including the transport of liquid components*

2025-18 Raimund Bürger, Enrique D. Fernández Nieto, José Garres-Díaz, Jorge Moya: *Well-balanced physics-based finite volume schemes for Saint-Venant-Exner-type models of sediment transport*

2025-19 Harold D. Contreras, Paola Goatin, Luis M. Villada: *Well-posedness of a nonlocal upstream-downstream traffic model*

2025-20 Thierry Coulbois, Anahi Gajardo, Pierre Guillon, Victor H. Lutfalla: *Aperiodic monotiles: from geometry to groups*

2025-21 Esteban Henriquez, Tonatiuh Sanchez-Vizuet, Manuel Solano: *An unfitted HDG discretization for a model problem in shape optimization*

Para obtener copias de las Pre-Publicaciones, escribir o llamar a: Director, Centro de Investigación en Ingeniería Matemática, Universidad de Concepción, Casilla 160-C, Concepción, Chile, Tel.: 41-2661324, o bien, visitar la página web del centro: `http://www.ci2ma.udec.cl`







Centro de Investigación en
Ingeniería Matemática (CI²MA)
Universidad de Concepción

Casilla 160-C, Concepción, Chile
Tel.: 56-41-2661324/2661554/2661316
http://www.ci2ma.udec.cl